

UC Irvine

UC Irvine Previously Published Works

Title

Two-photon absorption in silicon using the real density matrix approach

Permalink

<https://escholarship.org/uc/item/466304hj>

Journal

The Journal of Chemical Physics, 161(14)

ISSN

0021-9606

Authors

Ziemkiewicz, David

Knez, David

Garcia, Evan P

et al.

Publication Date

2024-10-14

DOI

10.1063/5.0219329












Copyright Information

This work is made available under the terms of a Creative Commons Attribution License, available at <https://creativecommons.org/licenses/by/4.0/>

Peer reviewed

RESEARCH ARTICLE | OCTOBER 11 2024

Two-photon absorption in silicon using the real density matrix approach

David Ziemkiewicz ; David Knez ; Evan P. Garcia ; Sylwia Zielińska-Raczyńska ;
Gerard Czajkowski ; Alessandro Salandrino ; Sergey S. Kharintsev ; Aleksei I. Noskov ;
Eric O. Potma ; Dmitry A. Fishman  



J. Chem. Phys. 161, 144117 (2024)

<https://doi.org/10.1063/5.0219329>



Articles You May Be Interested In

Pushing configuration-interaction to the limit: Towards massively parallel MCSCF calculations

J. Chem. Phys. (November 2017)



The Journal of Chemical Physics

Special Topics Open for Submissions

[Learn More](#)

Two-photon absorption in silicon using the real density matrix approach

Cite as: J. Chem. Phys. 161, 144117 (2024); doi: 10.1063/5.0219329

Submitted: 16 May 2024 • Accepted: 23 September 2024 •

Published Online: 11 October 2024



View Online



Export Citation



CrossMark

David Ziemkiewicz,¹ David Knez,² Evan P. Garcia,² Sylwia Zielińska-Raczyńska,¹
Gerard Czajkowski,¹ Alessandro Salandrino,³ Sergey S. Kharintsev,⁴ Aleksei I. Noskov,⁴
Eric O. Potma,² and Dmitry A. Fishman^{2,a)}

AFFILIATIONS

¹Institute of Mathematics and Physics, Technical University of Bydgoszcz, Al. Prof. S. Kaliskiego 7, 85-789 Bydgoszcz, Poland

²Department of Chemistry, University of California, Irvine, California 92697, USA

³Department of Electrical Engineering, University of Kansas, Lawrence, Kansas 66045, USA

⁴Institute of Physics, Kazan Federal University, Kazan 420008, Russia

^{a)}Author to whom correspondence should be addressed: dmitryf@uci.edu

ABSTRACT

Two-photon absorption in indirect gap semiconductors is a frequently encountered, but not well-understood phenomenon. To address this, the real-density matrix approach is applied to describe two-photon absorption in silicon through the excitonic response to the interacting fields. This approach produces an analytical expression for the dispersion of the two-photon absorption coefficient for indirect-gap materials and can be used to explain trends in reported experimental data for bulk silicon both old and new with minimal fitting.

Published under an exclusive license by AIP Publishing. <https://doi.org/10.1063/5.0219329>

I. INTRODUCTION

Two-photon absorption (2PA) is a nonlinear optical phenomenon in which the combined energy carried by two incident photons is near-instantaneously absorbed by a material. Because of its nonlinear intensity dependence, the 2PA process is spatially confined when focused light is used, thus making it possible to use the effect as a local probe in the material for imaging,¹ microfabrication,^{2,3} or three-dimensional data storage.⁴ In semiconducting materials, the 2PA phenomenon produces charge carriers that can be read out electronically, a mechanism that has been used extensively for measuring the envelopes of ultrashort optical pulses.^{5,6} The use of semiconductors as 2PA detectors is particularly attractive in the case of non-degenerate two-photon absorption (NTA), in which case the energies of $\hbar\omega_a$ and $\hbar\omega_b$ of the two photons in the interaction can be vastly different, enabling the registration of individual photon energies that are well below the bandgap energy of the semiconducting material. For instance, the NTA process has made it possible to detect mid-infrared (MIR) photons with wide-bandgap semiconductors, such as GaAs⁷ and Si,⁸ thereby circumventing thermal noise issues that have plagued traditional MIR photodetectors based on low-energy bandgap

materials. Moreover, the NTA principle has also been shown to enable rapid MIR imaging with high-definition visible/near-IR cameras,^{9–11} thereby overcoming several persistent limitations of conventional MIR cameras.

The recent developments in NTA-based imaging underline the potential of this nascent detection technology, particularly as it concerns the use of Si-based cameras for versatile imaging in the MIR range.^{9,11} From a commercial point of view, silicon is an attractive material because of its ubiquity as a feedstock and the mature technology for Si-device fabrication. On the other hand, silicon is an indirect semiconductor that has a much lower 2PA absorption coefficient compared to direct semiconductors in the same spectral range. The main reason for silicon's lower performance as a 2PA material is the additional involvement of lattice phonons for providing the momentum needed in the indirect transition, which lowers the transition probability.

Improving the 2PA response of Si-based photodetectors requires a better understanding of the indirect two-photon transition in silicon. Reasonable progress has been made in describing degenerate and non-degenerate two-photon absorption in *direct* bandgap semiconductors. Current models compute the 2PA transition rate in such materials through a second-order perturbation

of stationary material states,^{12–14} or via evolving Volkov-type wavefunctions in the context of first-order perturbation theory.¹⁵ These approaches have successfully produced expressions that generally predict the energy scaling of the two-photon absorption coefficient in direct bandgap materials, including the expected enhancement of the 2PA effect in the case of extremely non-degenerate photon energies.⁷ Existing models are flexible with respect to the input band structure but do not incorporate dephasing mechanisms explicitly, and extra care must be taken to account for material anisotropy.¹⁶ Alternative formulations include the use of semiconductor Bloch equations, which have been evaluated in the framework of the density operator that is better equipped to account for relaxation and dephasing mechanisms.^{17–19}

The description of 2PA in *indirect* semiconductors, such as silicon, has so far relied heavily on the theoretical models developed for direct bandgap materials. For instance, to account for the interaction vertex with lattice phonons, higher order perturbative expansions of stationary^{20,21} or dressed states²² have been developed to derive expressions for the nonlinear absorption coefficient. Although such models reproduce the general behavior of measured two-photon absorption coefficients, quantitative matching between experiment and theory has proven more challenging. Recently, Faryadraz *et al.* obtained a semi-empirical scaling law for NTA coefficients, which was compared with experimental data.²³ While semi-empirical models can be useful for gaining mechanistic insights, a more complete theory of two-photon absorption in indirect bandgap materials is needed to quantitatively predict the scaling of 2PA coefficients over a wide range of the energy ratio $\hbar\omega_b/\hbar\omega_a$.

In this work, we advance the theoretical description of the two-photon absorption process in silicon through the application of the real density matrix approach (RDMA). This approach has been successful in describing linear and nonlinear optical properties of semiconductors in terms of Rydberg excitons for the case of one-photon excitation.^{24,25} The RDMA method allows the use of a small number of well-known parameters (e.g., effective masses, gap energy, and dielectric constant) to derive expressions for the optical response of the material. Here, we adapt the RDMA for the case of two-photon excitation in semiconductors, extending it for the case of silicon to include both excitonic and continuum states, as well as lattice phonons for momentum matching. Using this approach, we derive analytical expressions for the two-photon coefficient while including dephasing times and anisotropy of the material under study. We compare the energy scaling of the predicted NTA coefficient with published experimental data, supplemented with new experimental data, and demonstrate excellent quantitative agreement over a broad range of $\hbar\omega_b/\hbar\omega_a$ dispersion values.

II. THEORY

A. Real density matrix approach

In this section, we briefly review the basic principles of the RDMA method in the context of linear and nonlinear optical excitations in semiconductors. In general, the optical response of semiconductors to incoming electromagnetic (EM) waves can be described in terms of the correlations in a many-body system (semiconductor) caused by the interactions between the EM fields, electrons, and holes (quasiparticles). A variety of theoretical methods has been used to describe the response, including Green's function approach^{26,27}

and the RDMA. The latter, also known as coherent wave theory or the band edge equations, was developed in works by Stahl *et al.*; see, for instance, Refs. 28 and 29.

In this work, we have chosen the RDMA to take advantage of its formulation in the real space. The method provides a direct relation between the density matrices and relevant observables, allowing an easy comparison between experimental and theoretical results. In general, the Coulomb interaction between the carriers in a many-body system produces an infinite hierarchy of evolution equations for n -point density matrices. The lowest level consists of two-point density matrices, which describe the interband transitions, between the valence and the conduction band, as well as the intraband transitions. Two-point density matrices are directly related to measurable quantities such as polarization and carrier densities, whereas higher order correlations are related, for example, to the formation of biexcitons.³⁰

Below, we restrict our model to two-point density matrices. The basic equations of the chosen approach are called the constitutive equations, or band-edge equations, and will be applied to describe the 2PA processes. We follow the description developed in Ref. 29. The RDMA takes into account the following contributions: (a) the electron-hole interaction, (b) the dipole interaction between the electron-hole pairs and the electromagnetic field. (c) the particle-surface interaction, and (d) the interaction between electron-hole pairs (excitons) and phonons. We consider a semiconductor in the real space representation, characterized by a number of valence and conduction bands. Electrons at site j in the conduction band are described by fermion operators \hat{c}_j^c (\hat{c}_j^c), which correspond to the creation (annihilation) operators. Similarly, operators \hat{d}_j^v (\hat{d}_j^v) are creation (annihilation) operators for holes in valence bands at site j . In the case of direct interband transitions, the Hamiltonian operator in our model consists of four parts,

$$H = H_0 + H_{em} + H_C + H_{ph}. \quad (1)$$

The term H_0 indicates the one-particle Bloch states in the conduction and valence bands and describes the intraband transport processes,

$$H_0 = \sum_{j\ell} \left(\sum_c T_{\ell j}^c \hat{c}_\ell^c \hat{c}_j^c - \sum_v T_{j\ell}^v \hat{d}_\ell^v \hat{d}_j^v \right), \quad (2)$$

where the transfer matrices $T_{ij}^{c,v}$ are given in terms of the band eigenvalues $E_{c,v}(k)$ as

$$\begin{aligned} T_{ij}^c &= \frac{1}{N} \sum_k e^{i\mathbf{k}(\mathbf{R}_i - \mathbf{R}_j)} E_c(\mathbf{k}) \\ T_{ij}^v &= \frac{1}{N} \sum_k e^{i\mathbf{k}(\mathbf{R}_i - \mathbf{R}_j)} E_v(\mathbf{k}) \end{aligned} \quad (3)$$

where \mathbf{R}_i and \mathbf{R}_j are lattice position vectors. The operator H_{em} describes the interaction with the electromagnetic field,

$$H_{em} = - \sum_{j\ell} \mathbf{E}_{j\ell} \cdot \sum_{cv} \mathbf{M}_{j\ell}^{cv*} \hat{d}_\ell^v \hat{c}_j^c + \text{h.c.}, \quad (4)$$

and $\mathbf{M}_{j\ell}^{cv}$ is the interband-dipole matrix element between Wannier states, which can be cast in the following form:

$$\mathbf{M}_{j\ell}^{cv} = \frac{1}{N} \sum_{\mathbf{k}} e^{i\mathbf{k}(\mathbf{R}_j - \mathbf{R}_\ell)} \mathbf{M}_{cv}(\mathbf{k}), \quad (5)$$

in terms of the dipole matrix element between Bloch functions,

$$\mathbf{M}_{cv}(\mathbf{k}) = -e \langle \psi_c(\mathbf{k}) | \mathbf{r} | \psi_v(\mathbf{k}) \rangle. \quad (6)$$

where $\mathbf{r} = \mathbf{r}_e - \mathbf{r}_h$ is the relative electron-hole coordinate. Here, we use the real-space version, i.e., Fourier transform, of Eq. (6),

$$\mathbf{M}_{\lambda,\mu}(\mathbf{r}) = \frac{e\hbar}{im_0(2\pi)^3} \int_{\text{BZ}} \frac{\mathbf{p}_{\lambda,\mu}(\mathbf{k}) e^{i\mathbf{k}\mathbf{r}}}{E_{c,\mu}(\mathbf{k}) - E_{v,\lambda}(\mathbf{k})} d^3k, \quad (7)$$

where $E_{c,v}(\mathbf{k})$ represents the energy of the band electrons, $\mathbf{p}_{\lambda,\mu}(\mathbf{k})$ is the momentum matrix element between Bloch states, and m_0 is the free electron mass. The integration extends over the first Brillouin zone. This form is chosen because all subsequent equations are expressed in the real-space representation. The electric field $\mathbf{E}_{j\ell}$ is considered at a mean point between the sites j and ℓ of the lattice; below, this position is assumed to coincide with the exciton center-of-mass. In the following, we assume the band structure is known from specific calculations.

The carrier interactions are described by the term H_C of the Hamiltonian,

$$H_C = \frac{1}{2} \sum_{i \neq j} V_{ij} (\hat{n}_i - \hat{h}_i) (\hat{n}_j - \hat{h}_j), \quad (8)$$

where the electron-hole interaction is screened by a background dielectric constant ϵ_b ,

$$V_{ij} = \frac{e^2}{4\pi\epsilon_0\epsilon_b|\mathbf{r}_i - \mathbf{r}_j|}, \quad (9)$$

where \mathbf{r}_i and \mathbf{r}_j are the electron and hole positions, respectively. Here, we define the electron and hole occupation numbers as

$$\hat{n}_j = \sum_c \hat{c}_j^\dagger \hat{c}_j, \quad \hat{h}_j = \sum_v \hat{d}_j^\dagger \hat{d}_j. \quad (10)$$

The free phonon Hamiltonian can be expressed as

$$H_{\text{ph}} = \sum_{\mu} \hbar\omega_{\mu} b_{\mu}^{\dagger} b_{\mu}, \quad (11)$$

where b_{μ}^{\dagger} and b_{μ} are the phonon creation and annihilation operators of mode μ with energy $\hbar\omega_{\mu}$.

The physical quantities relevant for finding the optical properties can be expressed in terms of mean values of the following pair operators:

$$\begin{aligned} \text{excitonic transition density amplitude: } Y_{12}^{ab} &= \langle \hat{Y}_{12}^{ab} \rangle = \langle \hat{a}_1^{\alpha} \hat{c}_2^{\beta} \rangle, \\ \text{electron density: } C_{12}^{ab} &= \langle \hat{C}_{12}^{ab} \rangle = \langle \hat{c}_1^{\alpha} \hat{c}_2^{\beta} \rangle, \\ \text{hole density: } D_{12}^{\alpha\beta} &= \langle \hat{D}_{12}^{\alpha\beta} \rangle = \langle \hat{a}_1^{\alpha} \hat{a}_2^{\beta} \rangle, \end{aligned} \quad (12)$$

where the indices a, b, \dots label the conduction bands, while α, β, \dots label the valence bands. The excitonic transition density Y_{12}^{ab} contributes to the interband transition polarization with the following term:

$$P = 2\text{Re} \left(\int_{r=r_1-r_2} d^3r \sum_{cv} M_{21}^{cv*} Y_{12}^{vc} \right), \quad (13)$$

and the diagonal elements (the matrices C and D) correspond to the densities of electrons,

$$\rho_e = -e \sum_c C_{12}^{cc} \Big|_{r_1=r_2}, \quad (14)$$

and holes,

$$\rho_h = e \sum_v D_{12}^{vv} \Big|_{r_1=r_2}. \quad (15)$$

The matrices above are sub-matrices of the following density matrix:

$$\underline{\hat{\rho}} = \begin{pmatrix} C_{cc'} & Y_{vc}^* \\ Y_{vc} & 1 - D_{v'v'} \end{pmatrix}. \quad (16)$$

The dynamics of the two-point matrices Y, C, D is part of the hierarchy of reduced density matrices and is obtained from the Heisenberg equations of motion,

$$i\hbar \partial_t \underline{\hat{\rho}} = [\underline{\hat{\rho}}, H] + i\hbar \partial_t \underline{\hat{\rho}}_{\text{irrev}}, \quad (17)$$

where the term $\underline{\hat{\rho}}_{\text{irrev}}$ describes the irreversible dissipation and radiation decay processes due to all dephasing processes. In this paper, we consider electron-electron interactions, electron-phonon interactions, and the optical transitions caused by the electromagnetic field. In many practical calculations, all irreversible processes are described in terms of two dephasing times T_1, T_2 , which are taken as phenomenological constants that satisfy the following equation:

$$\frac{\partial \underline{\hat{\rho}}}{\partial t} \Big|_{\text{irrev}} = - \left(\begin{array}{cc} \frac{1}{T_1} [C(t) - C^{(0)}] & \frac{1}{T_2} [Y^*(t) - Y^{*(0)}] \\ \frac{1}{T_2} [Y(t) - Y^{(0)}] & \frac{1}{T_1} [D(t) - D^{(0)}] \end{array} \right). \quad (18)$$

where the states with superscript (0) denote the steady-state solutions. Although silicon is an indirect bandgap semiconductor, the valence and conduction bands near the fundamental critical points can be effectively approximated by paraboloids.³¹ Therefore, in our current model, the Hamiltonian in Eq. (17) employs parabolic bands. This Hamiltonian is derived from Eq. (1) by averaging the relevant operators and can be expressed as follows:

$$H = H_{ee} + H_{hh} + H_{eh} + H_{\text{ex-ph}} \quad (19)$$

where the electron Hamiltonian,

$$H_{ee} = \frac{1}{2m_e} [(p_2 + eA_2)^2 - (p_1 - eA_1)^2] + e(\Phi_1^e - \Phi_2^e), \quad (20)$$

the hole Hamiltonian,

$$H_{hh} = \frac{1}{2m_h} [(p_2 - eA_2)^2 - (p_1 + eA_1)^2] - e(\Phi_1^h - \Phi_2^h) \quad (21)$$

and the electron–hole interaction,

$$H_{eh} = E_g - V_{12} + \frac{1}{2m_h}(p_1 - eA_1)^2 + \frac{1}{2m_e}(p_2 + eA_2)^2 + e(\Phi_1^h - \Phi_2^e), \quad (22)$$

where E_g denotes the gap energy, m_e, m_h are the effective masses of electrons and holes, respectively, $-V_{12}$ is the statically screened Coulomb potential, M_0 is the element in Eq. (5) integrated over the real space, A_j is the vector potential of the EM at position \mathbf{r}_j , which may include an external magnetic field, $\Phi_j^{e/h}$ is the scalar, external, or electromagnetically induced potential acting on electrons (or holes) at position \mathbf{r}_j , and E_j denotes the electric field of the radiation at the point \mathbf{r}_j . We neglect for the moment the vectorial and tensorial indices and use the common notation for the momentum operators: $p_1 = -i\hbar\nabla_1$, etc. The electron–electron, hole–hole, and electron–hole exchange terms are included in the third term of the Hamiltonian (1), as given by expression (8), and are obtained by means of the random phase approximation (RPA) decoupling scheme.³²

The Hamiltonian H_{ph} (11) is expressed using creation and annihilation operators. In line with the RDMA approach, we have replaced it with H_{ex-ph} , the Hamiltonian corresponding to exciton–phonon interaction, formulated in real space as

$$H_{ex-ph} = a(\mathbf{q}) e^{-i\omega_{ph}t} V_p(\mathbf{q}, \mathbf{r}) + \text{c.c.}, \quad (23)$$

with

$$V_p(\mathbf{q}, \mathbf{r}) = \sum_{\mathbf{R}_a} \left(\frac{\hbar}{2M\omega_{ph}} \right)^{1/2} e^{i\mathbf{q}\cdot\mathbf{R}_a} \mathbf{e}_0 \nabla_r V(\mathbf{r} - \mathbf{R}_a). \quad (24)$$

where ω_{ph} is the angular phonon frequency and \mathbf{q} is its wave vector. The $a(\mathbf{q})$ is the phonon annihilation operator (with corresponding momentum $\hbar\mathbf{q}$ and energy $\hbar\omega_{ph}$), its adjoint is the phonon creation operator, $V(\mathbf{r} - \mathbf{R}_a)$ is the potential at the point \mathbf{R}_a , and \mathbf{e}_0 is the phonon polarization.

With the above expressions, the Heisenberg Eq. (17) becomes a closed set of differential equations (“constitutive equations”) for Y, C, D , which can be obtained in explicit form using the following procedure:^{33,34}

- (i) setting up the Heisenberg equations of motion for the pair operators,
- (ii) applying anti-commutation rules for the Fermion operators $\hat{c}_j^\dagger, \hat{c}_j, \hat{d}_j^{\dagger v},$ and \hat{d}_j^v to bring all operator products into normal order,
- (iii) computing the expectation values of the relevant operators,
- (iv) using an interpolation procedure to obtain a continuum dependence on the position variables (for example, Ref. 34),
- (v) making use of the RPA to factorize four-point density matrices.

As a result, we obtain the constitutive equations for the interband transition density amplitudes, which for any couple of bands are of the following form:

$$\begin{aligned} & -i\hbar\partial_t Y_{12} + H_{eh} Y_{12} + X_{12}^Y \\ & = M_0(E\delta_{12} - E_1 C_{12} - E_2 D_{21}) - i\hbar \left(\frac{\partial Y_{12}}{\partial t} \right)_{\text{irrev}}, \end{aligned} \quad (25)$$

with X_{12}^Y being the electron–hole exchange term, while the last dissipative term is responsible for irreversible excitation transfers. For intraband transitions (time dependence of the population of the band states), we obtain

$$-i\hbar\partial_t C_{12} + H_{ee} C_{12} + X_{12}^C = -M_0(E_1 Y_{12} - E_2 Y_{21}^*) - i\hbar \left(\frac{\partial C_{12}}{\partial t} \right)_{\text{irrev}}, \quad (26)$$

$$-i\hbar\partial_t D_{12} + H_{hh} D_{12} + X_{12}^D = -M_0(Y_{21} E_1 - Y_{12}^* E_2) - i\hbar \left(\frac{\partial D_{12}}{\partial t} \right)_{\text{irrev}}, \quad (27)$$

where X_{12}^C and X_{12}^D are the electron–electron and hole–hole exchange terms, respectively. We note that the relaxation processes incorporated here are characterized by the condition $T_1 \gg T_2$. This implies that phonons remain in equilibrium during the creation/annihilation of excitons. The numerical subscripts are abbreviations for the coordinates, such as in $Y_{12} = Y(\mathbf{r}_1, \mathbf{r}_2)$, etc. The exchange terms X^Y, X^C, X^D read

$$\begin{aligned} X_{12}^Y &= \frac{i}{\hbar} \int d^3 r (V_{12} - V_{23})(Y_{13} C_{32} - D_{31} Y_{23}), \\ X_{12}^C &= \frac{i}{\hbar} \int d^3 r (V_{13} - V_{23})(Y_{31}^* Y_{32} + C_{13} C_{32}), \\ X_{12}^D &= \frac{i}{\hbar} \int d^3 r (V_{13} - V_{23})(Y_{31}^* Y_{32} + D_{13} D_{32}), \end{aligned} \quad (28)$$

where V_{12} is the statistically screened Coulomb potential.³⁵ It can be seen that those terms represent four-point correlations but are not taken into account for two-point correlation functions. It should be stressed that Hamiltonians are bilocal—they are defined in $(\mathbf{r}_1, \mathbf{r}_2)$ space.

The electromagnetic fields \mathbf{A}, \mathbf{E} , and Φ that appear in (21) and (22) are self-consistent fields that include the induced contributions produced by the sources and those contained in Y, C, D . The spatial dependence of the functions Y, C, D in the constitutive equations refers to a macroscopic scale. Microscopic structures can be taken into account by an appropriate choice of the parameters, as, for example, effective masses and M_0 in expressions (25)–(27). The above expressions must be solved simultaneously with the Maxwell field equations,

$$-c^2 \epsilon_0 \nabla \times \nabla \times \mathbf{E} - \epsilon_0 \epsilon_b \ddot{\mathbf{E}} = \ddot{\mathbf{P}}, \quad (29)$$

where the polarization is given by expression (13), and c is the speed of light. A theoretical scheme containing higher order correlations has been presented in Ref. 36, which also discusses phonon-assisted transitions.

As mentioned above, the term H_{ph} in the Hamiltonian (19) describes the electron–crystal lattice interaction. Using perturbation calculus, we obtain the matrix elements of H_{eh} , under the condition of momentum conservation, and that of H_{ph} , which involves transfer of a specific momentum \mathbf{q} . The calculated transition probability per unit time of a process in which the valence electron is

scattered to the conduction state ψ_{ck_2} , and a photon of energy $\hbar\omega$ with a phonon of momentum $\mathbf{q} = \mathbf{k}_1 - \mathbf{k}_2$ and energy $\hbar\omega_{\mathbf{q}}$ are both absorbed, which gives the absorption coefficient in the case of the phonon absorption,³⁷

$$\alpha_{\text{ph,abs}}(\omega) = \begin{cases} 0, & \text{for } \hbar\omega < E_g - \hbar\omega_{\text{ph}} \\ C_1(\hbar\omega - E_g + \hbar\omega_{\text{ph}})^2 n_{\mathbf{q}}, & \text{for } \hbar\omega > E_g + \hbar\omega_{\text{ph}} \end{cases}, \quad (30)$$

where $n_{\mathbf{q}}$ is the phonon occupation number representing the number of available phonons with wave vector \mathbf{q} , and C_1 is a constant. By considering all values of \mathbf{q} corresponding to energy $\hbar\omega_{\text{ph}}$, we use the distribution

$$n_{\text{ph}}(\omega_{\text{ph}}) = \frac{1}{\exp\left(\frac{\hbar\omega_{\text{ph}}}{k_B \mathcal{T}}\right) - 1}, \quad (31)$$

where k_B is the Boltzmann constant, and \mathcal{T} is the temperature. The absorption coefficient in the case of phonon emission is given by

$$\alpha_{\text{ph,em}}(\omega) = \begin{cases} 0, & \hbar\omega < E_g + \hbar\omega_{\text{ph}} \\ C_1(\hbar\omega - E_g - \hbar\omega_{\text{ph}})^2 n_{\text{ph}}, & \hbar\omega > E_g + \hbar\omega_{\text{ph}} \end{cases}, \quad (32)$$

The case of exciton formation in an indirect transition can be illustrated as follows. Following the discussion above, let us consider the case of parabolic non-degenerate energy bands with a maximum of the valence band at $\mathbf{k} = 0$, and a minimum of the conduction band at $\mathbf{k} = \mathbf{q}_0$, with the dispersion,

$$E_c(\mathbf{k}_e) = \frac{\hbar^2(\mathbf{k}_e - \mathbf{q}_0)^2}{2m_e^*} + E_g, \quad E_v(\mathbf{k}_h) = -\frac{\hbar^2\mathbf{k}_h^2}{2m_h^*}. \quad (33)$$

For $k_{\text{ex}} = q_0$, we obtain possible exciton energies,

$$E_{\text{ex}}(q_0) = E_g - |E_{n\ell mH}|, \quad (34)$$

[see also Eq. (48)] for states below the energy gap and a continuum for states above the indirect gap. The absorption coefficients due to indirect exciton transitions in a process in which a photon and a phonon are simultaneously absorbed, and for the lowest exciton state, are given by

$$\alpha_{\text{ph,abs}}(\omega) = \begin{cases} 0 & \text{for } \hbar\omega < E_g - E_1 - \hbar\omega_{\text{ph}}, \\ C_2(\hbar\omega - E_g + E_1 + \hbar\omega_{\text{ph}})^{1/2} n_{\text{ph}} & \text{for } \hbar\omega > E_g - E_1 - \hbar\omega_{\text{ph}}. \end{cases} \quad (35)$$

where C_2 is a constant,³⁷ and we have written $E_1 = |E_{100H}|$. The analogous expression for the absorption coefficient under the emission of a phonon has the following form:

$$\alpha_{\text{ph,em}}(\omega) = \begin{cases} 0 & \text{for } \hbar\omega < E_g - E_1 + \hbar\omega_{\text{ph}}, \\ C_2(\hbar\omega - E_g + E_1 - \hbar\omega_{\text{ph}})^{1/2} n_{\text{ph}} & \text{for } \hbar\omega > E_g - E_1 + \hbar\omega_{\text{ph}}. \end{cases} \quad (36)$$

The total contribution of phonons to the absorption is then given by

$$\alpha_{\text{ph,total}} = \alpha_{\text{ph,abs}}(\omega) + \alpha_{\text{ph,em}}(\omega). \quad (37)$$

It can be seen from the above expressions that the effect of phonons is relevant when considering continuum states.

As discussed in Refs. 38 and 39, the phonon density of states contains two local maxima at 20 and 60 meV, with a weighted average of $\sim\hbar\omega_{\text{ph}} = 40$ meV. This simplified approach of taking an estimate of the average phonon energy provides a good fit to experimental data. In the same manner, as mentioned above, an integration of $n_{\mathbf{q}}$ over all of the values of \mathbf{q} yields an average phonon number n_{ph} that can be used in Eqs. (30)–(36).

B. Two-photon absorption

We next adapt the described RDMA approach to the case of two-photon absorption. We assume that static external fields are absent, thus neglecting the vector potential A and the scalar potential Φ^{el} in the Hamiltonian expressions (21) and (22). In expressions (25)–(27), the electromagnetic field \mathbf{E} now includes two frequencies ω_a and ω_b and is written as

$$\mathbf{E} = \mathbf{E}_{0a} \exp(i\mathbf{k}_a \mathbf{R} - i\omega_a t) + \mathbf{E}_{0b} \exp(i\mathbf{k}_b \mathbf{R} - i\omega_b t) + \text{c.c.}, \quad (38)$$

where

$$|\mathbf{k}_j| = \frac{\omega_j}{c} \sqrt{\epsilon(\omega_j)} = n_j \frac{\omega_j}{c}, \quad j = a, b, \quad (39)$$

and n_j are refractive indices at the frequencies ω_j and \mathbf{R} is the electron–hole pair center-of-mass coordinate,

$$\mathbf{R} = \mathbf{R}_{12} = \frac{m_h \mathbf{r}_1 + m_e \mathbf{r}_2}{m_h + m_e}. \quad (40)$$

The linear optical properties are calculated by solving the interband Eq. (25), supplemented by the corresponding Maxwell equation, where the polarization (13) acts as a source. For computing the nonlinear optical properties, we use the entire set of constitutive Eqs. (25) and (26). Although finding a general solution of the equations is challenging, in special situations, a solution can be found. For example, if one assumes that the matrices Y , C , and D can be expanded in powers of the electric field \mathbf{E} , an iterative procedure can be used.

In general, solving for Y , C , and D in the context of two-photon absorption depends on the relation between the incoming frequencies ω_a, ω_b (and thus energies $\hbar\omega_a, \hbar\omega_b$) and the fundamental gap energy E_g , which enters as a parameter in the electron–hole Hamiltonian. We consider two relevant cases to be discussed separately.

1. When $\hbar\omega_a + \hbar\omega_b < 2E_g$, the excitation of discrete excitonic states is possible. Therefore, we seek solutions in terms of eigenfunctions and eigenvalues of the electron–hole Hamiltonian, taking also into account the phonons.
2. In the energy range $\hbar\omega_a + \hbar\omega_b > 2E_g$, we solve Eqs. (44) and (77) and the following equations for the matrices C, D assuming $V_{12} = 0$,²⁴ thus entering the energy range represented by continuum states. The solution is obtained in terms of appropriate Green's function.

C. Discrete states—linear susceptibility

Our goal is to derive expressions for the NTA absorption coefficients. These can be obtained from the third-order nonlinear susceptibility, which, in turn, can be determined via an iterative procedure within the context of the RDMA. The first step in the iteration consists of solving Eq. (25), which at this stage takes on the following form:

$$i\hbar\partial_t Y^{(1)} - H_{ch} Y^{(1)} = -\mathbf{M}\mathbf{E} + i\hbar\left(\frac{\partial Y^{(1)}}{\partial t}\right)_{\text{irrev}}. \quad (41)$$

For the irreversible part, we assume the following simple form:

$$\left(\frac{\partial Y^{(1)}}{\partial t}\right)_{\text{irrev}} = -\frac{1}{T_2} Y^{(1)}. \quad (42)$$

In the discussion of nonlinear effects, we also take into account the non-resonant parts of the amplitude Y . The excitonic density Y will consist of two parts, Y_a, Y_b , as defined by the angular frequencies ω_a and ω_b . In addition, due to the valence band structure of the semiconducting material (Si), we must consider heavy-hole (H) and light-hole (L) excitons. Considering optical transitions between the (H, L) valence bands and the conduction band, with the mentioned inclusion of both the resonant and anti-resonant parts, Eq. (12) generates eight equations: a pair for amplitude Y_{aH} : $Y_{aH}^{(1)} \propto \exp(-i\omega_a t)$ and for $Y_{aH+}^{(1)} \propto \exp(i\omega_a t)$, as follows:

$$i\hbar\left(i\omega_a + \frac{1}{T_2}\right)Y_{aH+}^{(1)} - H_{ch} Y_{aH+}^{(1)} = -\mathbf{M}_H \mathbf{E}_a^*(\mathbf{R}, t), \quad (43)$$

$$i\hbar\left(-i\omega_a + \frac{1}{T_2}\right)Y_{aH-}^{(1)} - H_{ch} Y_{aH-}^{(1)} = -\mathbf{M}_H \mathbf{E}_a(\mathbf{R}, t), \quad (44)$$

with similar equations for $Y_{bH\pm}^{(1)}$, where \mathbf{M}_H is the transition dipole density. Analogous equations hold for the amplitudes $Y_{a,bL\pm}^{(1)}$, with the appropriate transition dipole density \mathbf{M}_L . In the following, we consider only one component of the vectors \mathbf{E} , \mathbf{P} , and \mathbf{M} , and focus our attention on the heavy hole exciton transition.

For the case of discrete exciton states, the exciton density in the first step is found as

$$Y_{daH-}^{(1)} = E_a(\mathbf{R}, t) \sum_{n\ell m} \frac{c_{n\ell mH} \Phi_n(\mathbf{r})}{\hbar(\Omega_{n\ell mH} - \omega_a - i/T_2)}, \quad (45)$$

$$Y_{daH+}^{(1)} = E_a^*(\mathbf{R}, t) \sum_{n\ell m} \frac{c_{n\ell m} \Phi_{n\ell mH}(\mathbf{r})}{\hbar(\Omega_{n\ell mH} + \omega_a - i/T_2)},$$

and similar expressions for $Y_{dbH\pm}^{(1)}$. The subscript “d” indicates the case of discrete excitonic states. The expansion coefficients are defined as follows:

$$\begin{aligned} c_{n\ell mH} &= \int d^3 r M_H(\mathbf{r}) \varphi_{n\ell mH}(\mathbf{r}), \\ \hbar\Omega_{n\ell mH} &= \hbar\Omega_{n\ell m} = E_g + E_{n\ell mH}(\gamma_{aH}), \\ \varphi_{n\ell mH} &= R_{n\ell H}(r) Y_{\ell m}(\theta, \phi), \end{aligned} \quad (46)$$

where $R_{n\ell H}$ are the hydrogen radial functions of the anisotropic Schrödinger equation,⁴⁰

$$r = \sqrt{x^2 + y^2 + \frac{z^2}{\gamma_{aH}}}, \quad (47)$$

where $Y_{\ell m}(\theta, \phi)$ are the spherical harmonics, and $E_{n\ell mH}$ are the corresponding eigenvalues,

$$E_{n\ell mH} = -\frac{\eta_{\ell mH}(\gamma_{aH}) R_H^*}{n^2}, \quad n = 1, 2, \dots, \quad \ell = 0, 1, 2, \dots, n-1, \\ m = 0, 1, 2, \dots, \ell, \quad (48)$$

where R_H^* is the effective excitonic Rydberg energy for the heavy hole exciton,

$$R_H^* = \frac{\mu_{\parallel H} e^4}{2(4\pi\epsilon_0 \sqrt{\epsilon_{\parallel} \epsilon_z})^2 \hbar^2}, \quad (49)$$

and the anisotropy parameter γ_{aH} is defined as

$$\gamma_{aH} = \frac{\mu_{\parallel H} \epsilon_{\parallel}}{\mu_{zH} \epsilon_z},$$

where $\mu_{\parallel H}$ and μ_{zH} are the heavy hole exciton reduced masses in the x - y plane and in the z -direction, respectively,

$$\frac{1}{\mu_{\parallel H}} = \frac{1}{m_{e\parallel}} + \frac{1}{m_{h\parallel H}}, \quad \frac{1}{\mu_{zH}} = \frac{1}{m_{ez}} + \frac{1}{m_{hzH}}. \quad (50)$$

The anisotropic electron and heavy hole masses (in-plane and in the z -direction) are listed in Table I, where ϵ_0 is the vacuum dielectric constant, and $\epsilon_{\parallel}, \epsilon_z$ are relative dielectric tensor elements. The quantity $\eta_{\ell mH}(\gamma_{aH})$ is given by the following expression:

$$\eta_{\ell mH}(\gamma_{aH}) = \int_0^{2\pi} d\phi \int_0^{\pi} \frac{|Y_{\ell m}|^2 \sin \theta d\theta}{\sqrt{\sin^2 \theta + \gamma_{aH} \cos^2 \theta}}. \quad (51)$$

In what follows, we consider only the excitonic s states, with $\ell = m = 0$, and denote

$$\begin{aligned} \varphi_{n00H} &= \varphi_{nH}, \quad c_{n00H} = c_{nH}, \quad E_{n00H} = E_{nH}, \\ \hbar\Omega_{n00H} &= \hbar\Omega_{nH} + E_n(\gamma_{aH}). \end{aligned} \quad (52)$$

It should be noted that at room temperature, accounting for the relatively low binding energy of excitons in Si (15 meV as in Ref. 41), only the lowest excitonic state is relevant, so we set $n = 1$.

The solutions for $Y_{da,b\pm}^{(1)}$ determined above permit the calculation of the linear polarization,

$$\begin{aligned} P_H^{(1)}(\omega) &= \int d^3 r \left[Y_{daH-}^{(1)} + Y_{daH+}^{(1)*} \right] M_H^*(\mathbf{r}) \\ &\quad + \int d^3 r \left[Y_{dbH-}^{(1)} + Y_{dbH+}^{(1)*} \right] M_H^*(\mathbf{r}) \\ &= \frac{E_{0a}}{\hbar} \frac{2|c_{1H}|^2 \Omega_{1H}}{\Omega_{1H}^2 - (\omega_a + i/T_2)^2} + \frac{E_{0b}}{\hbar} \frac{2|c_{1H}|^2 \Omega_{1H}}{\Omega_{1H}^2 - (\omega_b + i/T_2)^2} \\ &= \epsilon_0 \chi_{dH}^{(1)}(\omega_a) E_{0a} + \epsilon_0 \chi_{dH}^{(1)}(\omega_b) E_{0b}. \end{aligned} \quad (53)$$

The susceptibilities defined in Eq. (53) can be expressed in terms of the band parameters and, for energies below the gap, when spatial dispersion is neglected, we obtain

TABLE I. Band parameter values for Si, masses in free electron mass m_0 , H denotes heavy-hole, and L light-hole, R_{HL}^* is calculated from $(\mu_{\parallel HL}/\varepsilon_b^2) \times 13\,600$ meV, a_{HL}^* is calculated from $(1/\mu_{\parallel HL})\varepsilon_b \times 0.0529$ nm, and $m_{e,dos}$ (density-of-state effective mass) is calculated from $6^{2/3}(m_{e\parallel}m_{e\parallel}m_{e_z})^{1/3}$.

Parameter	Value (4.2 K)	Value (300 K)	Unit	References
E_g	1170	1124	meV	43
Δ_{LTH}	0.1		meV	
R_H^*	15	16.56	meV	
R_L^*	7.94	9.6	meV	
γ_1	4.285	2.45		44
γ_2	0.339	0.194		44
γ_3	1.446	0.826		44
m_{ez}	0.9163	1.09	m_0	45
$m_{e\parallel}$	0.1905	0.2	m_0	45
$m_{e,dos}$	1.06	1.16	m_0	
m_{hzH}	0.28	0.485	m_0	Equation (102), ⁴⁶
$m_{h\parallel H}$	0.72	1.25	m_0	Equation (102)
m_{hzL}	0.2	0.35	m_0	
$m_{h\parallel L}$	0.14	0.24	m_0	
μ_{zH}	0.214	0.336	m_0	
$\mu_{\parallel H}$	0.15	0.172	m_0	
μ_{zL}	0.164	0.26	m_0	
$\mu_{\parallel L}$	0.08	0.1	m_0	
a_H^*	4.13	3.66	nm	
a_L^*	7.74	6.3	nm	
r_{0H}	0.46	0.44	nm	
r_{0L}	0.64	0.58	nm	
ε_b	11.7	11.9		
T_2	0.1		ns	41
T_1	8		ns	Fitting
$\hbar\omega_{ph}$	40		meV	Fitting ³⁹

$$\chi_{dH}^{(1)}(\omega_j) = \varepsilon_b \frac{f_{1H}\Delta_{LTH}/R_H^*}{(E_{T1H} - \hbar\omega_j - i\hbar/T_2)/R_H^*}, \quad (54)$$

where $j = a, b$, and E_{T1H} is the energy of the first heavy hole exciton resonance. For the dipole density $M_H(\mathbf{r})$ described by the following formula:

$$M_H(\mathbf{r}) = M_{0H} \frac{1}{\sqrt{4\pi}} \frac{1}{r} \frac{1}{r_{0H}^2 a_H^*} e^{-r/r_{0H}} Y_{00}(\theta, \phi), \quad (55)$$

where $r_{0H} = (2\mu_{\parallel H}E_g/\hbar^2)^{-1/2}$ is the so-called coherence radius, the anisotropy-dependent oscillator strength f_{1H} has the following form:

$$f_{1H} = \frac{\eta_{00H}^3(1 - \eta_{00H}r_{0H}/a_H^*)}{(1 + \eta_{00H}r_{0H}/a_H^*)^4}, \quad (56)$$

where a_H^* is the heavy hole effective excitonic Bohr radius,

$$a_H^* = \frac{4\pi\hbar^2\varepsilon_0\sqrt{\varepsilon_{\parallel}}\varepsilon_z}{\mu_{\parallel H}e^2}. \quad (57)$$

The longitudinal transverse splitting of the ground state is²⁹

$$\frac{\Delta_{LTH}}{R^*} = 2 \frac{2\mu_{\parallel H}}{\varepsilon_0\varepsilon_b\pi a_H^*\hbar^2} M_{0H}^2, \quad (58)$$

where the above mentioned bulk dielectric constant is given by $\varepsilon_b = \sqrt{\varepsilon_z\varepsilon_{\parallel}}$ and is $f_n\Delta_{LTH}$ for the excited states ($n > 1$). Treating Δ_{LTH} as a known quantity, the above relation allows computation of the dipole matrix element M_{0H} .

D. Discrete states–nonlinear susceptibility

To obtain the nonlinear response, the solutions for $Y_{daH,b\pm}^{(1)}$ are inserted as a source term in the conduction band Eq. (26) and the valence band Eq. (27). Note that each of these equations depends on the electromagnetic field. If the irreversible terms are well defined, Eqs. (26) and (27) can be solved, and this second step of the iteration yields expressions for the density matrices C_H and D_H . We use for the irreversible terms a linear relaxation time approximation,

$$\left(\frac{\partial C}{\partial t}\right)_{\text{irrev}} = -\frac{1}{\tau} [C(\mathbf{X}, \mathbf{r}, t) - f_{0e}(\mathbf{r})C(\mathbf{X}, \mathbf{r} = 0, t)] - \frac{C(0)}{T_1}, \quad (59)$$

where $\mathbf{X} = (\mathbf{r}_1 + \mathbf{r}_2)/2$, τ is the carrier relaxation time, and f_{0e}, f_{0h} are normalized Boltzmann distributions for electrons and holes, respectively,

$$f_{0e}(\mathbf{r}) = \int d^3q f_{0e}(\mathbf{q}) e^{-i\mathbf{q}\mathbf{r}} = \exp\left(-\frac{m_{e\parallel}k_B\mathcal{F}}{2\hbar^2}\rho^2 - \frac{m_{ez}k_B\mathcal{F}}{2\hbar^2}z^2\right), \quad (60)$$

The same type of expression holds for the holes. The diagonal elements of the matrices are related to charge densities (14) and (15), which are conserved quantities. Therefore, we assume that they relax to an equilibrium normalized to the actual number of carriers. The relaxation time T_1 stands for the interband recombination time.⁴² Using the irreversible terms (59) in the intraband Eqs. (26) and (27), and looking for stationary solutions, we obtain the matrices C, D in the following form:

$$C_H(\mathbf{r}) = -\frac{i}{\hbar} [\tau J_{CH}(\mathbf{r}) - \tau J_{CH}(0) + T_1 f_{0e}(\mathbf{r}) J_{CH}(0)],$$

$$D_H(\mathbf{r}) = -\frac{i}{\hbar} [\tau J_{HH}(\mathbf{r}) - \tau J_{HH}(0) + T_1 f_{0hH}(\mathbf{r}) J_{HH}(0)],$$

where

$$J_{CH} = \frac{2iM_0|E_{0a}|^2}{\hbar} [\text{Im } g_H(-\omega_a, \mathbf{r}) + \text{Im } g_H(\omega_a, \mathbf{r})] + \frac{2iM_0|E_{0b}|^2}{\hbar} [\text{Im } g_H(-\omega_b, \mathbf{r}) + \text{Im } g_H(\omega_b, \mathbf{r})], \quad (61)$$

and

$$g_H(\pm\omega_j, \mathbf{r}) = \sum_n \frac{c_{nH}\varphi_{nH}(\mathbf{r})}{\Omega_{nH} \mp \omega_j - i/T_2}, \quad (62)$$

with $J_{CH} = J_{DH}$. These density matrices can then, in turn, be used as a source term for Eq. (25), which can be solved to obtain expressions for $Y_{da,bH\pm}^{(3)}$ in the final step of the iteration.

The equations for the third-order coherent amplitudes $Y_{jH\pm}^{(3)}$ now take on the following form:

$$i\hbar\left(i\omega_a + \frac{1}{T_2}\right)Y_{aH+}^{(3)} - H_{eh}Y_{aH+}^{(3)} = M_{0H}(E^*C_H + E^*D_H) = E^*(\mathbf{R}, t)\tilde{J}_H, \quad (63)$$

$$i\hbar\left(-i\omega_a + \frac{1}{T_2}\right)Y_{aH-}^{(3)} - H_{eh}Y_{aH-}^{(3)} = M_{0H}(E^*C_H + E^*D_H) = E^*(\mathbf{R}, t)\tilde{J}_H, \quad (64)$$

with similar equations for $Y_{bH\pm}^{(1)}$, where

$$\tilde{J}_H = -\frac{i}{\hbar}M_{0H}[T_1J_{CH}(0)f_{0eH}(\mathbf{r}) + T_1J_{VH}(0)f_{0hH}(\mathbf{r})].$$

Once $Y_{aH\pm}^{(3)}$ and $Y_{bH\pm}^{(3)}$ are known, the third-order polarization can be determined as

$$P_H^{(3)}(\omega) = \int d^3r[Y_{aH-}^{(3)} + Y_{aH+}^{(3)*}]M_H^*(\mathbf{r}) + \int d^3r[Y_{bH-}^{(3)} + Y_{bH+}^{(3)*}]M_H^*(\mathbf{r}). \quad (65)$$

We consider nonlinear polarizations at the same frequency ω (or frequencies in the case 2PA) as that of an incident field, which means that we consider the susceptibilities $\chi^{(1)}$ and $\chi^{(3)}$ related to the excitonic amplitudes $Y^{(1)}$ and $Y^{(3)}$, respectively.

Similar to the approach presented in Sec. II A, to account for the presence of phonons, we separate the polarization related to the emission of a phonon (subscript “em”) and the absorption of a phonon (subscript “abs”). The emission contribution has the following form:

$$P_{dH,em}^{(3)}(\omega_a, \omega_b) = P_{daH,em}^{(3)}e^{-i\omega_a t} + P_{dbH,em}^{(3)}e^{-i\omega_b t}, \quad (66)$$

where the polarization amplitudes are defined by

$$P_{daH,em}^{(3)} = \varepsilon_0\chi_{dH,self,em}^{(3)}(\omega_a, \omega_a)|E(\omega_a)|^2 E(\omega_a) + \varepsilon_0\chi_{dH,cross,em}^{(3)}(\omega_a, \omega_b)|E(\omega_b)|^2 E(\omega_a),$$

$$P_{dbH,em}^{(3)} = \varepsilon_0\chi_{dH,self,em}^{(3)}(\omega_b, \omega_b)|E(\omega_b)|^2 E(\omega_b) + \varepsilon_0\chi_{dH,cross,em}^{(3)}(\omega_b, \omega_a)|E(\omega_a)|^2 E(\omega_b),$$

The nonlinear susceptibilities have the following form:

$$\chi_{dH,self,em}^{(3)}(\omega_j, \omega_j) = -(n_{ph} + 1)\frac{2M_{0H}^2}{\varepsilon_0}\frac{1}{T_2}\left(T_1 + \frac{i\hbar\delta(\omega - 2\omega_j)}{\hbar\omega + i\hbar/T_1}\right) \times \sum_{\ell} \frac{c_{\ell H}(A_{\ell H} + B_{\ell H})\hbar\Omega_{\ell H,em}}{(\hbar\Omega_{\ell H,em})^2 - (\hbar\omega_j + i\hbar T_2^{-1})^2} \times \sum_n \frac{c_{nH}\varphi_{nH}(0)}{(\hbar\Omega_{nH,em} - \hbar\omega_j)^2 + (\hbar/T_2)^2}, \quad (67)$$

$$\chi_{dH,cross,em}^{(3)}(\omega_a, \omega_b) = -(n_{ph} + 1)\frac{2M_{0H}^2}{\varepsilon_0}\left(\frac{T_1}{T_2}\right) \times \sum_{\ell} \frac{c_{\ell H}(A_{\ell H} + B_{\ell H})\hbar\Omega_{\ell H,em}}{(\hbar\Omega_{\ell H,em})^2 - (\hbar\omega_a + i\hbar T_2^{-1})^2} \times \sum_n \frac{c_{nH}\varphi_{nH}(0)}{(\hbar\Omega_{nH,em} - \hbar\omega_b)^2 + (\hbar/T_2)^2}. \quad (68)$$

The additional cross term $\chi_{dH,cross,em}^{(3)}(\omega_b, \omega_a)$ is obtained by permuting the frequencies ω_a and ω_b in Eq. (66). The expressions $\hbar\Omega_{nH,em,abs}$ are the exciton resonance energies that include the phonon energies $\hbar\omega_{ph}$,

$$\hbar\Omega_{nH,em,abs} = E_g + E_{nH} \pm \hbar\omega_{ph}, \quad (69)$$

where “+” stands for phonon emission and “−” for phonon absorption. The coefficients $A_{\ell H}, B_{\ell H}$ in Eq. (67) appearing in the expressions for $Y_{da,bH\pm}^{(3)}$ have the following form:

$$A_{\ell H} = \int d^3r \varphi_{\ell H}(\mathbf{r}) f_{0e}(\mathbf{r}) = \int d^3r \varphi_{\ell H}(\mathbf{r}) \exp\left(-\frac{\rho^2}{2\lambda_{th,e}^2} - \frac{z^2}{2\lambda_{th,eZ}^2}\right), \quad (70)$$

$$B_{\ell H} = \int d^3r \varphi_{\ell H}(\mathbf{r}) f_{0hH}(\mathbf{r}) = \int d^3r \varphi_{\ell H}(\mathbf{r}) \exp\left(-\frac{\rho^2}{2\lambda_{th,hH}^2} - \frac{z^2}{2\lambda_{th,hZH}^2}\right),$$

where $\lambda_{th,e}, \lambda_{th,hH}$ are the so-called thermal lengths for electrons and holes, respectively,

$$\lambda_{th,e} = \left(\frac{\hbar^2}{m_e k_B \mathcal{T}}\right)^{1/2}, \quad \lambda_{th,hH} = \left(\frac{\hbar^2}{m_h k_B \mathcal{T}}\right)^{1/2}, \quad (71)$$

determined for the appropriate masses (\parallel or z). The above expressions are valid when $\hbar\omega < E_g + \hbar\omega_{ph}$. For $\hbar\omega > E_g + \hbar\omega_{ph}$, one should replace $n_{ph} + 1$ by

$$\mathcal{C}(\hbar\omega - E_g - \hbar\omega_{ph})^2 (n_{ph} + 1). \quad (72)$$

where \mathcal{C} is a constant.³⁷

Analogous expressions can be obtained for the susceptibilities that include phonon absorption,

$$\chi_{dH,self,abs}^{(3)}(\omega_j, \omega_j) = -n_{ph}\frac{2M_0^2}{\varepsilon_0}\frac{1}{T_2}\left(T_1 + \frac{i\hbar\delta(\omega - 2\omega_j)}{\hbar\omega + i\hbar/T_1}\right) \times \sum_{\ell} \frac{c_{\ell}(A_{\ell H} + B_{\ell H})\hbar\Omega_{\ell H,abs}}{(\hbar\Omega_{\ell H,abs})^2 - (\hbar\omega_j + i\hbar T_2^{-1})^2} \times \sum_n \frac{c_{nH}\varphi_{nH}(0)}{(\hbar\Omega_{nH,abs} - \hbar\omega_j)^2 + (\hbar/T_2)^2}, \quad (73)$$

$$\begin{aligned} \chi_{\text{dH,cross,abs}}^{(3)}(\omega_a, \omega_b) &= -n_{\text{ph}} \frac{2M_{0H}^2}{\epsilon_0} \left(\frac{T_1}{T_2} \right) \\ &\times \sum_{\ell} \frac{c_{\ell H}(A_{\ell H} + B_{\ell}) \hbar \Omega_{\ell H, \text{abs}}}{(\hbar \Omega_{\ell H, \text{abs}})^2 - (\hbar \omega_a + i\hbar T_2^{-1})^2} \\ &\times \sum_n \frac{c_{nH} \varphi_{nH}(0)}{(\hbar \Omega_{nH, \text{abs}} - \hbar \omega_b)^2 + (\hbar/T_2)^2}, \end{aligned} \quad (74)$$

plus the additional cross term $\chi_{\text{dH,cross,abs}}^{(3)}(\omega_b, \omega_a)$ obtained by permuting the input frequencies in (74). The above expressions are valid when

$$\hbar \omega < E_g - \hbar \omega_{\text{ph}}.$$

Otherwise, n_{ph} should be replaced by

$$\mathcal{E}(\hbar \omega - E_g + \hbar \omega_{\text{ph}})^2 n_{\text{ph}}. \quad (75)$$

In Sec. II F, we use the expressions for the nonlinear susceptibility above to determine the nonlinear absorption coefficients in silicon.

E. Continuum states

In this section, we consider the case relevant to heavy-hole exciton transitions. If $(\hbar \omega - \hbar \omega_{\text{ph}}) > E_g$ for the case of phonon emission, or $(\hbar \omega + \hbar \omega_{\text{ph}}) > E_g$ for the case of phonon absorption, then there is no generation of bound exciton states, and continuum states constitute the final states instead. In this case, $Y_H^{(1)}$ is calculated in the first iteration step by setting $V_{12} = 0$ in the electron-hole Hamiltonian,²⁴ giving rise to equations of the following form:

$$\left(E_g \pm \hbar \omega \pm \hbar \omega_{\text{ph}} - i \frac{\hbar}{T_2} - \frac{\hbar^2}{2\mu_{\parallel H}} \nabla^2 \right) Y_{H\pm} = \mathbf{M}_H(\mathbf{r}) \mathbf{E}. \quad (76)$$

Equation (76) can be solved by means of appropriate Green's function,

$$Y_{H\pm}^{(1)} = \int d^3 r' g_{H\pm}(r, r') \mathbf{M}_H(r', \theta, \phi) \mathbf{E}, \quad (77)$$

where

$$g_{H\pm}(r, r') = \frac{2\mu_{\parallel H}}{\hbar^2} \frac{\sinh \kappa_{H\pm} r^{\lessgtr}}{4\pi \kappa_{H\pm} r^{\lessgtr}} e^{-\kappa_{H\pm} r^{\lessgtr}}, \quad (78)$$

$r^{\lessgtr} = \min(r, r')$ and $r^{\gtr} = \max(r, r')$, and

$$\kappa_{H\pm}^2 = \frac{2\mu_{\parallel H}}{\hbar^2} \left(E_g \pm \hbar \omega \pm \hbar \omega_{\text{ph}} - i \frac{\hbar}{T_2} \right). \quad (79)$$

Assuming a linear polarization and the wave vector \mathbf{E} having a component E_0 in a direction α , simultaneously with the dipole density \mathbf{M}_H having a component M_{0H} in the same direction and, for simplicity, using the dipole density of the following form:

$$M_H(\mathbf{r}) = \frac{M_{0H} \delta(r - r_{0H})}{4\pi r_{0H}^2}, \quad (80)$$

we obtain

$$Y_{H\pm}^{(1)} = M_{0H} E_0 g_{H\pm}(r, r_{0H}). \quad (81)$$

We may again define amplitudes of the form $Y_{caH\pm}^{(1)}, Y_{cbH\pm}^{(1)}$, where the subscript “c” now indicates the involvement of continuum states. If, in the case of phonon emission, we encounter $\kappa_H^2 < 0$, and introduce

$$\kappa_H = -i\tilde{\kappa}_H, \quad (82)$$

where

$$\tilde{\kappa}_{H-}^2 = \frac{2\mu_{\parallel H}}{\hbar^2} \left(\hbar \omega - \hbar \omega_{\text{ph}} - E_g + i \frac{\hbar}{T_2} \right),$$

and, in this case, Green's function takes on the following form:

$$g_{H-}(r, r') = \frac{2\mu_{\parallel H}}{\hbar^2} \frac{\sin \tilde{\kappa}_{H\pm} r^{\lessgtr}}{4\pi \tilde{\kappa}_{H\pm} r^{\lessgtr}} e^{i\tilde{\kappa}_{H\pm} r^{\lessgtr}}. \quad (83)$$

The linear terms for the case of phonon emission and absorption and input frequency ω_a are found as

$$\begin{aligned} Y_{caH-,em}^{(1)}(r) &= M_{0H} E_0 a g_{aH-,em}(r, r_{0H}), Y_{caH-,abs}^{(1)}(r) \\ &= M_{0H} E_0 a g_{aH-,abs}(r, r_{0H}), \end{aligned} \quad (84)$$

with

$$\begin{aligned} g_{aH-,em}(r, r_{0H}) &= \frac{2\mu_{\parallel H}}{\hbar^2} \frac{\sin(\tilde{\kappa}_{aH-,em} r^{\lessgtr})}{4\pi \tilde{\kappa}_{aH-,em} r r_{0H}} e^{i\tilde{\kappa}_{aH-,em} r^{\lessgtr}}, \\ \tilde{\kappa}_{aH-,em}^2 &= \frac{2\mu_{\parallel H}}{\hbar^2} [\hbar \omega_a - (E_g + \hbar \omega_{\text{ph}})] + i \frac{2\mu_{\parallel H}}{\hbar^2} \frac{\hbar}{T_2}. \end{aligned}$$

Similar expressions can be obtained for the amplitudes at input frequencies ω_b . The linear amplitudes, thus, are obtained from the source for calculating the C_H and D_H matrices, followed by the third step to determine $Y_{ca,bH\pm}^{(3)}$, similar to the procedure described in Sec. II C. Once the $Y_{ca,bH\pm}^{(3)}$ amplitudes are found, for both the phonon emission and absorption process, we may write the nonlinear cross susceptibility for the continuum states as

$$\chi_{\text{cH,cross}}^{(3)} = \chi_{\text{cH,cross,em}}^{(3)}(\omega_a, \omega_b) + \chi_{\text{cH,cross,abs}}^{(3)}(\omega_a, \omega_b), \quad (85)$$

with

$$\begin{aligned} \chi_{\text{cH,cross,em}}^{(3)}(\omega_a, \omega_b) &= -(n_{\text{ph}} + 1) \frac{2}{\epsilon_0} \frac{T_1}{\hbar} M_{0H}^4 \left(\frac{2\mu_{\parallel H}}{\hbar^2} \right)^2 \\ &\times \frac{1}{4\pi r_{0H}} \left(\frac{\sin(\tilde{\kappa}_{aH-,em} r_{0H})}{\tilde{\kappa}_{aH-,em} r_{0H}} \right)^2 \\ &\times [\tilde{\kappa}_{bH-,em} r_{0H} + \tilde{\kappa}_{bH-,abs} r_{0H}] \\ &\times (\mathcal{A}_{eH,em} + \mathcal{B}_{hH,em}), \end{aligned} \quad (86)$$

$$\begin{aligned} \chi_{\text{cH,cross,abs}}^{(3)}(\omega_a, \omega_b) &= -n_{\text{ph}} \frac{2}{\epsilon_0} \frac{T_1}{\hbar} M_{0H}^4 \left(\frac{2\mu_{\parallel H}}{\hbar^2} \right)^2 \\ &\times \frac{1}{4\pi r_{0H}} \left(\frac{\sin(\tilde{\kappa}_{aH-,abs} r_{0H})}{\tilde{\kappa}_{aH-,abs} r_{0H}} \right)^2 \\ &\times [\tilde{\kappa}_{bH-,em} r_{0H} + \tilde{\kappa}_{bH-,abs} r_{0H}] \\ &\times (\mathcal{A}_{eH,abs} + \mathcal{B}_{hH,abs}), \end{aligned} \quad (87)$$

where

$$\begin{aligned}\tilde{\kappa}_{jH-,em}r_{0H} &= \left(x_j - \frac{E_g + \hbar\omega_{ph}}{E_g}\right)^{1/2}, \\ \tilde{\kappa}_{j-,abs}r_{0H} &= \left(x_j - \frac{E_g - \hbar\omega_{ph}}{E_g}\right)^{1/2}, \\ x_j &= \frac{\hbar\omega_j}{E_g}.\end{aligned}\quad (88)$$

Here, $\mathcal{A}_{eH,em}$, $\mathcal{B}_{hH,em}$, $\mathcal{A}_{eH,abs}$, $\mathcal{B}_{hH,abs}$ are the continuum counterparts to expressions (70), appropriate for discrete states. Making use of the relations (70), we obtain

$$\begin{aligned}\mathcal{A}_{eH,em} &= \mathcal{A}'_{eH,em} + i\mathcal{A}''_{eH,em} = \frac{2\mu_{\parallel H} \sin(\tilde{\kappa}_{aH-,em}r_{0H})}{\hbar^2 \tilde{\kappa}_{aH-,em}r_{0H}} \\ &\times \int_{\rho_{0H}}^{\infty} \rho \, d\rho \int_0^{\infty} dz \frac{\exp(-i\tilde{\kappa}_{aH-,em}z) \sqrt{\rho^2 + (z^2/\gamma_{aH})}}{\sqrt{\rho^2 + (z^2/\gamma_{aH})}} \\ &\times \exp\left(-\frac{\rho^2}{2\lambda_{th,e\parallel}^2} - \frac{z^2}{2\lambda_{th,e\perp}^2}\right),\end{aligned}\quad (89)$$

with an analogous expression for $\mathcal{A}_{eH,abs}$, $\mathcal{B}_{hH,em}$, and $\mathcal{B}_{hH,abs}$. The value $\rho_{0H} = r_{0h}/a_H^*$.

F. Nonlinear absorption coefficients

The propagation of the field components E_{0a} and E_{0b} in the semiconductor follows from the wave equation with $P^{(3)}$ as a source term, which, after making the well-known slowly varying amplitude approximation, yield the following coupled equations for the field amplitudes:

$$\begin{aligned}\frac{\partial E_{0a}}{\partial z} &= i \frac{\omega_a}{n_a c} \chi_{\text{selfH}}^{(3)}(\omega_a, \omega_a) |E_{0a}|^2 E_{0a} \\ &+ i \frac{\omega_a}{n_a c} \chi_{\text{crossH}}^{(3)}(\omega_a, \omega_b) |E_{0b}|^2 E_{0a},\end{aligned}\quad (90)$$

$$\begin{aligned}\frac{\partial E_{0b}}{\partial z} &= i \frac{\omega_b}{n_b c} \chi_{\text{selfH}}^{(3)}(\omega_b, \omega_b) |E_{0b}|^2 E_{0b} \\ &+ i \frac{\omega_b}{n_b c} \chi_{\text{crossH}}^{(3)}(\omega_b, \omega_a) |E_{0a}|^2 E_{0b}.\end{aligned}\quad (91)$$

From the equation above, the intensities of the input beams can be found as

$$I_a = 2\varepsilon_0 n_a c |E_{0a}|^2, \quad \frac{\partial I_a}{\partial z} = 2\varepsilon_0 n_a c \left[E_{0a}^* \frac{\partial E_{0a}}{\partial z} + E_{0a} \frac{\partial E_{0a}^*}{\partial z} \right]. \quad (92)$$

Similar expressions are obtained for I_b , resulting in the following set of coupled Eqs. (90) and (91), and we obtain the set of equations:

$$\frac{\partial I_a}{\partial z} = -\alpha_2(\omega_a, \omega_a) I_a^2(z) - \alpha_2(\omega_a, \omega_b) I_a(z) I_b(z), \quad (93)$$

$$\frac{\partial I_b}{\partial z} = -\alpha_2(\omega_b, \omega_b) I_b^2(z) - \alpha_2(\omega_b, \omega_a) I_b(z) I_a(z),$$

These equations define the nonlinear absorption coefficients α_2 as

$$\begin{aligned}\alpha_{2H}(\omega_a, \omega_a) &= \frac{\omega_a}{2\varepsilon_0 n_a^2 c^2} \chi_{\text{selfH}}^{(3),I}(\omega_a, \omega_a), \\ \alpha_{2H}(\omega_a, \omega_b) &= \frac{\omega_a}{2\varepsilon_0 n_a n_b c^2} \chi_{\text{crossH}}^{(3),I}(\omega_a, \omega_b), \\ \alpha_{2H}(\omega_b, \omega_a) &= \frac{\omega_b}{2\varepsilon_0 n_a n_b c^2} \chi_{\text{crossH}}^{(3),I}(\omega_b, \omega_a), \\ \alpha_{2H}(\omega_b, \omega_b) &= \frac{\omega_b}{2\varepsilon_0 n_b^2 c^2} \chi_{\text{selfH}}^{(3),I}(\omega_b, \omega_b),\end{aligned}\quad (94)$$

where $\chi_H^{(3),I}$ indicates the imaginary part of $\chi_H^{(3)}$. The refractive indices $n_a = n(\omega_a)$, $n_b = n(\omega_b)$ are defined by the real parts of the linear susceptibility $\chi^{(1)}$, written as

$$n_a = \left\{ \left[\varepsilon_b \left(1 + \frac{f_1 \Delta_{LT} [\hbar\Omega_{n,em}/E_g - x_a]}{[(\hbar\Omega_{n,em}/E_g) - x_a]^2 + \gamma_2^2} \right) \right] \right\}^{1/2}, \quad (95)$$

with analogous formulas for ω_b and the absorptive term $\hbar\Omega_{n,abs}$. Here, $\gamma_2 = \hbar/(E_g T_2)$, f_1 is the oscillator strength (here for the heavy hole exciton), written as

$$f_{1H} = \frac{\eta_{00H}^3}{[1 + \eta_{00H}(r_{0H}/a_H^*)]^3}, \quad (96)$$

see Eq. (56).

The susceptibilities and, consequently, the nonlinear absorption coefficients, are composed of four components: two corresponding to the contributions of discrete and continuous states, and each of them containing terms related to phonon emission and absorption,

$$\alpha_{2H}(\omega_a, \omega_b) = \alpha_{2dH}(\omega_a, \omega_b) + \alpha_{2cH}(\omega_a, \omega_b). \quad (97)$$

For the discrete states, we only consider the lowest exciton state with $n = 1$, yielding the following form:

$$\begin{aligned}\alpha_{2dH}(\omega_a, \omega_b) &= -2x_a \gamma_2 \alpha' \left(\frac{T_1}{T_2} \right) \left\{ \frac{\varepsilon_b}{n_a n_b} \frac{n_{ph} + 1}{(\hbar\Omega_{1H,em}/E_g - x_b)^2 + \gamma_2^2} \right. \\ &\times \frac{\hbar\Omega_{1H,em}/E_g}{[(\hbar\Omega_{1H,em}/E_g)^2 - x_a^2]^2 + (2\gamma_2 x_a)^2} \\ &+ \frac{\varepsilon_b}{n_a n_b} \frac{n_{ph}}{(\hbar\Omega_{1H,abs}/E_g - x_a)^2 + \gamma_2^2} \\ &\left. \times \frac{\hbar\Omega_{1H,abs}/E_g}{[(\hbar\Omega_{1H,abs}/E_g)^2 - x_b^2]^2 + (2\gamma_2 x_b)^2} \right\},\end{aligned}\quad (98)$$

where the constant α' is defined as

$$\begin{aligned} \alpha'_H(\omega_a, \omega_b) &= 2 \frac{4E_g}{\varepsilon_0 \hbar n_a n_b 2c^2 E_g^3} \frac{2M_{0H}^2}{\varepsilon_0} [\varphi_{1H}(0)A_{1H} + \varphi_{1H}(0)B_{1H}] c_{1H}^2 \\ &= 2 \frac{1}{4} \varepsilon_0^2 \varepsilon_b^2 \pi^2 a_{1H}^{*6} \Delta_{LTH}^2 \times \frac{4}{\pi \varepsilon_0 \hbar n_a n_b c^2 E_g^2} \\ &\quad \times [\varphi_{1H}(0)A_{1H} + \varphi_{1H}(0)B_{1H}] \left(\frac{\eta_{00H}}{a_{1H}^*} \right)^3 \frac{1}{(1 + \eta_{00H} r_{0H} / a_{1H}^*)^2} \\ &= 2 \frac{\pi \varepsilon_b^2 \Delta_{LTH}^2 (\eta_{00H} a_{1H}^*)^3}{E_g^2 \hbar c^2 n_a n_b} \frac{[\varphi_{1H}(0)A_{1H} + \varphi_{1H}(0)B_{1H}]}{(1 + \eta_{00H} r_{0H} / a_{1H}^*)^2}. \end{aligned}$$

The continuum states contribution has the following form:

$$\alpha_{2cH}(\omega_a, \omega_b) = \alpha_{2cH,em}(\omega_a, \omega_b) + \alpha_{2cH,abs}(\omega_a, \omega_b), \quad (99)$$

where

$$\begin{aligned} \alpha_{2cH,em}(\omega_a, \omega_b) &= - \frac{4E_g (n_{ph} + 1)}{\varepsilon_0 \hbar n_a n_b c^2} M_{0H}^4 \left(\frac{2\mu_{\parallel H}}{\hbar^2} \right)^2 \frac{1}{4\pi r_{0H}} \frac{T_1}{\hbar} \\ &\quad \times x_a \left(\frac{\sin(\tilde{\kappa}_{aH-,em} r_{0H})}{\tilde{\kappa}_{aH-,em} r_{0H}} \right)^2 [\tilde{\kappa}_{bH-,em} r_{0H} + \tilde{\kappa}_{bH-,abs} r_{0H}] \\ &\quad \times (\mathcal{A}'_{eH,em} + \mathcal{B}'_{hH,em}), \end{aligned} \quad (100)$$

and

$$\begin{aligned} \alpha_{2cH,abs}(\omega_a, \omega_b) &= - \frac{4E_g n_{ph}}{\varepsilon_0 \hbar n_a n_b c^2} M_{0H}^4 \left(\frac{2\mu_{\parallel H}}{\hbar^2} \right)^2 \frac{1}{4\pi r_{0H}} \frac{T_1}{\hbar} \\ &\quad \times x_a \left(\frac{\sin(\tilde{\kappa}_{aH-,abs} r_{0H})}{\tilde{\kappa}_{aH-,abs} r_{0H}} \right)^2 [\tilde{\kappa}_{bH-,em} r_{0H} + \tilde{\kappa}_{bH-,abs} r_{0H}] \\ &\quad \times (\mathcal{A}''_{eH,abs} + \mathcal{B}''_{hH,abs}). \end{aligned} \quad (101)$$

The solutions obtained in the two regimes of discrete and continuous states are smoothly connected via the use of hyperbolic tangent functions. Using the above formula, we have calculated the 2PA coefficient $\alpha_2(\omega_a, \omega_b)$ as a function of the energies $\hbar\omega_a + \hbar\omega_b$. The band parameters used in the calculations are listed in Tables I–III.

The masses are calculated from Luttinger parameters,

TABLE II. Anisotropy parameters for Si and excitonic energies calculated from Eq. (48).

Parameter	Value (4.2 K)	Value (300 K)	Unit	Reference
γ_{aH}	0.7	0.51		Equation (51)
η_{00H}	1.058	1.1		Equation (51)
$ E_{10H} $	16.79	20	meV	

TABLE III. Thermal electron and hole lengths for Si and expressions $\varphi_{1H}(0)A_{1H}, \varphi_{1H}(0)B_{1H}$.

Quantity	Value 4.2 K	Value 300 K	Reference
$\bar{\lambda}_{th,e\parallel}$	8.08	1.05	Equation (103)
$\bar{\lambda}_{th,e\perp}$	3.68	0.45	Equation (103)
$\bar{\lambda}_{th,h\parallel H}$	4.15	0.42	Equation (103)
$\bar{\lambda}_{th,h\perp H}$	6.66	0.67	Equation (103)
$\varphi_{1H}(0)A_{1H}$	4×1.52	4×0.173	
$\varphi_{1H}(0)B_{1H}$	4×1.34	4×0.06	

$$\begin{aligned} m_{hzH} &= \frac{m_0}{\gamma_1 - 2\gamma_2}, \\ m_{h\parallel H} &= \frac{m_0}{\gamma_1 - 2\gamma_3}, \\ m_{hzL} &= \frac{m_0}{\gamma_1 + 2\gamma_2}, \\ m_{h\parallel L} &= \frac{m_0}{\gamma_1 + 2\gamma_3}. \end{aligned} \quad (102)$$

With the reduced electron and hole masses, the thermal lengths are given by

$$\begin{aligned} \bar{\lambda}_{th,e} &= \left(\frac{\hbar^2}{m_{e\parallel} k_B \mathcal{F}} \right)^{1/2} = \left(2 \times \frac{\hbar^2}{2\mu_{\parallel H}} \times \frac{\mu_{\parallel H}}{m_{e\parallel}} \frac{1}{k_B \mathcal{F}} \right)^{1/2} \\ &= \left(2 \times \frac{\mu_{\parallel H}}{m_{e\parallel}} \frac{R_H^*}{k_B \mathcal{F}} \right)^{1/2}, \bar{\lambda}_{th,hH} = \left(\frac{\hbar^2}{m_{h\parallel} k_B \mathcal{F}} \right)^{1/2} k_B T \\ &= 8.617 \times 10^{-2} \frac{\text{meV}}{\text{K}}. \end{aligned} \quad (103)$$

The calculated values are summarized in Table III.

III. EXPERIMENTAL

We perform optical experiments to determine nonlinear absorption coefficients of silicon to supplement existing data in the literature, spanning a wider range of $x = \frac{\hbar(\omega_a + \omega_b)}{2E_g}$ values. For this purpose, we perform cross-correlation experiments, using optical pulses derived from a 1 kHz amplified femtosecond laser system (Spitfire Ace, Spectra Physics). The laser seeds two optical parametric amplifiers (OPA, TOPAS-Prime, Light Conversion), where one OPA is used as a source of near-infrared (NIR) probe radiation between 1150 and 1350 nm (1.08–0.91 eV), producing pulses in the range of 100–150 fs. The signal and idler pulses from the second OPA system are used to generate MIR pump pulses through the process of difference frequency generation (DFG) in the 2480–4651 nm (0.5–0.27 eV) range, producing 175–265 fs pulses. The MIR pump is modulated using an optical chopper at a frequency of 500 Hz that is synchronized to the laser output (MC2000B, Thorlabs).

We use a 280 μm thick [100] silicon window (99.999% purity, University Wafer) as the sample target. The MIR and NIR pulses are focused in a non-collinear arrangement on the Si target, using normal incidence for the pump beam and a $\sim 20^\circ$ incidence angle for the probe beam. Temporal overlap is controlled through an automated translation stage (GTS150, Newport) in the probe arm, producing a

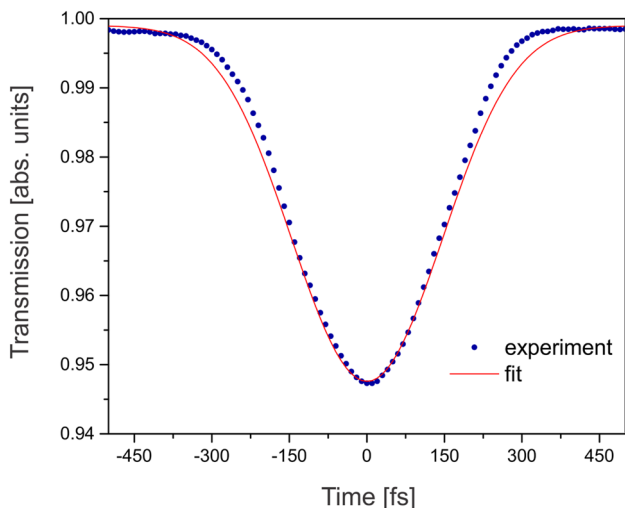


FIG. 1. Exemplary pump–probe data and corresponding nonlinear transmittance fit. The photon energies used here are 0.91 and 0.376 eV.

TABLE IV. Experimentally obtained values for α_2 in cm/GW.

Wavelength (nm)	2480	3295	3755	4220
1150	1.099	0.71	0.823	0.955
1200	0.951	0.638	0.705	0.817
1250	0.846	0.564	0.501	0.481
1350	0.634	0.452	0.385	0.307

cross-correlation of pump-induced probe absorption via NTA. The remaining probe is attenuated by an OD = 3 neutral density filter and detected using a home-built InGaAs photodiode. The modulated change induced by the MIR pump is analyzed by a lock-in amplifier (SR860, Stanford Research Systems). The resulting cross-correlation is then used to extract the nonlinear absorption coefficient α_2 as described by Negres *et al.*⁴⁷

Figure 1 shows a representative cross-correlation and its corresponding fit, and the tabulated data of extracted α_2 values are presented in Table IV. A full description of the data analysis is presented in the supplementary material. Pump-to-probe beam radius ratios were maintained to at least 8:1 as measured by knife edge scan. The low irradiance of the probe beam in conjunction with the use of a lock-in amplifier ensures that any degenerate two-photon absorption present is excluded from the measured signal. The pump beam is always the longer wavelength beam, minimizing free carrier absorption induced by the probe via three- or four-photon absorption.

IV. RESULTS AND DISCUSSION

The derived form of α_{2H} that follows from the RDMA contains contributions from the two regimes of exciton production, namely, the contributions from discrete states and continuum states, see Eq. (97). The discrete regime is visually depicted in Fig. 2, which

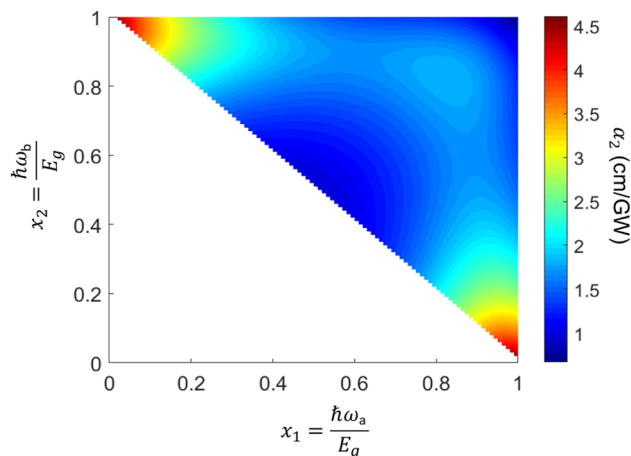


FIG. 2. Scaling behavior of the two-photon absorption coefficient α_2 [Eq. (103)] as a function of normalized photon energy while both photons are below the gap.

highlights the two-dimensional dispersion of α_2 . The analysis recognizes the presence of a single discrete excitonic state below the band edge, corresponding to the creation of a bound state through the absorption of a phonon, $\hbar\Omega_{abs}$, which may provide considerable enhancement to the 2PA process. This is manifested by the presence of resonant denominators for the discrete regime, which can be written in a simplified form from Eq. (98) as

$$\alpha_{2dH}(\omega_a, \omega_b) \propto \frac{1}{(\hbar\Omega_{abs}/E_g - \hbar\omega_b/E_g)^2 + \gamma_2^2} \times \frac{\hbar\Omega_{em}/E_g}{[(\hbar\Omega_{em}/E_g)^2 - (\hbar\omega_a)^2]^2 + (2\gamma_2\hbar\omega_a)^2} \quad (104)$$

This single state is the only one considered due to the low binding energy of Si, which precludes the formation of bound excitons with higher principal quantum numbers. When $\hbar\omega_b/\hbar\omega_a$ is detuned away from degeneracy, we observe an increase of α_2 that is as much as 5× the equivalent degenerate response, amplifying the process as it becomes doubly resonant with the lowest discrete state and the edge of the continuum at room temperature. This behavior is evident in the corners of Fig. 2. While smaller in magnitude, the $\hbar\Omega_{abs}$ state provides additional enhancement when at least one incident photon approaches this energy. An alternate resonance condition exists when both photons are resonant with the discrete exciton level at ~95% of the band gap. This is a singly resonant process where the intermediate state is the lowest excitonic state, providing some enhancement to the two-photon process.

If the energy of the incident photons exceeds the bandgap energy, then the two-photon absorption process proceeds entirely via continuum states. This can be accessed by either phonon absorption or emission, and the nonlinear absorption coefficient has the form as in Eq. (99). Beyond the band edge, the continuum causes α_{2cH} to further increase up to the point where the energy of at least one of the photons has enough energy to reach the direct gap of silicon at $E_g = 3.43$ eV. This increase is due to the oscillatory behavior of the linear coherent amplitude of the exciton density $Y^{(1)}$, which

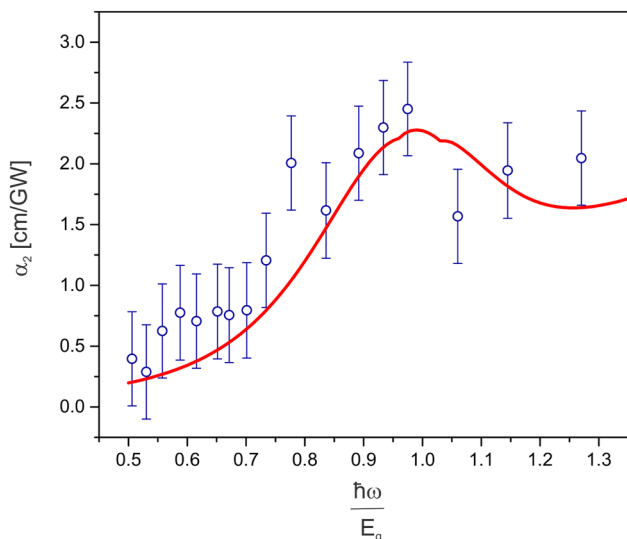


FIG. 3. Scaling of the degenerate two-photon absorption coefficient α_2 as a function of $x = \hbar\omega/E_g$. Squares are obtained from Ref. 48 and thick solid line results from the RDMA analysis of two-photon absorption.

contributes to the induced polarization of the medium in order for two-photon absorption to occur.

To validate the performance of the model, we first apply it to explain an experimental data set of the degenerate two-photon (DTA) cross section obtained from an open aperture Z-scan reported in Ref. 48. As shown in Fig. 3(a), α_2 for the DTA process reveals a resonance-like behavior as a function of photon energy. A previous analysis using a model for direct transitions, corrected for the center of mass energy when phonon scattering is involved,⁴⁹ reproduced the general dependence of α_2 on the photon energy, but it failed to predict the observed resonance structure. The RDMA approach (indicated by the solid line in Fig. 3), on the other hand, predicts a resonant behavior when the individual photon energy approaches the energy of the discrete exciton state, resulting in a satisfactory description of the data. When the photon energy exceeds the bandgap, the role of the bound exciton states decreases, and instead, the response is largely dictated by continuum states, which results in a slight decrease of α_2 . Note that only the dephasing times in the RDMA analysis are fitting parameters, while all other parameters are obtained from the tabulated values given in Tables I–III.

We next use the model to describe the energy scaling of the NTA coefficient as measured in Ref 23, which encompasses photons with an energy ratio from 1.6 to 2.08 (Fig. 4). In addition, we have performed measurements using pump photon energies of 0.294–0.5 eV and probe energies of 0.91–1.08 eV, corresponding to the photon energy ratio from 1.82 to 3.67 (Fig. 5). Together, these two sets of measurements cover a wide range of energy ratios (1.6–3.7), offering a robust dataset for validating our model.

We observe that the RDMA predictions for α_2 are in good agreement with both experimental datasets. The most notable feature in the normalized photon energy curve is the appearance of a

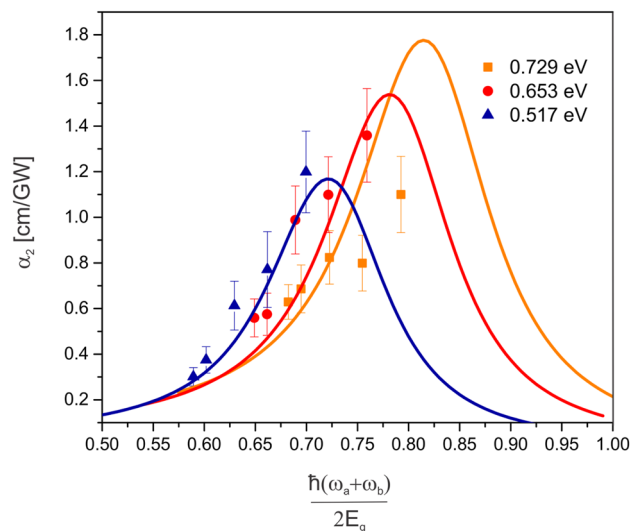


FIG. 4. Scaling of the non-degenerate two-photon absorption coefficient α_2 as a function of the normalized equivalent energy. Experimental data points are obtained from Ref. 23 and thick solid lines represent the results from the RDMA analysis. Different colors correspond to different photon energies $\hbar\omega_a$.

peak, which the model attributes to the presence of the bound exciton resonance. The position of this peak shifts in accordance with the energy tuning of the lower energy pump photon, and its magnitude is largely dictated by the damping terms in the resonant denominators of α_{2dH} . However, this resonant behavior is significantly different from what is reported in Ref. 23, where the theoretical predictions anticipate a quasi-linear scaling of α_2 as a function of the

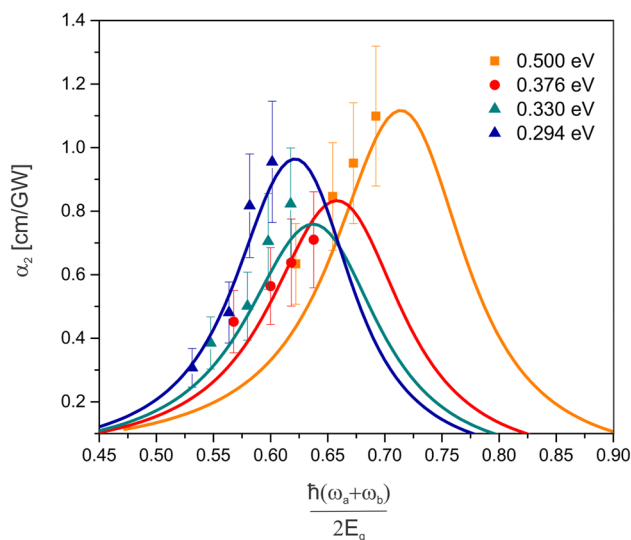


FIG. 5. Scaling of the non-degenerate two-photon absorption coefficient α_2 as a function of the normalized equivalent energy. Data points indicate experimental results obtained in this study, and thick solid lines represent the results from the RDMA analysis. Different colors correspond to different photon energies $\hbar\omega_a$.

normalized photon energy. Future work may include NTA experiments to verify the behavior of α_2 and the influence of continuum states above the band edge, such as can be obtained with a two-color Z-scan.

This work is a significant departure from the conventional understanding of the two-photon absorption process in semiconductors. Previous methods have described the 2PA absorption process in terms of transition rate matrix elements based on electron band states, where significantly non-degenerate photon pairs become resonant with the interband transition and an intraband transition simultaneously. Within the framework of the RDMA, the defining feature of the absorption process is the ability to produce either bound or free excitons within the material. Tracking the formation of excitons allows the RDMA to yield general expressions for semiconducting materials with low binding energies, i.e., only the lowest discrete state needs to be considered. These results are analytical in that there is no parametrization done to provide free variables for fitting. The only variability results from loosely determined material parameters, namely the relaxation times T_1 and T_2 .

It is possible to apply this analysis to direct gap two-photon transitions as well, which omits the involvement of phonon absorption or emission processes in the final equations. The RDMA also accounts for the physical realities of material anisotropy and relaxation mechanisms that are often added phenomenologically elsewhere. Bolstered by the excellent agreement between theory and experiment over a wide range of photon energies and non-degeneracy ratios, we believe that the current description provides a deeper insight into two-photon absorption process in semiconducting materials.

V. CONCLUSION

We have employed the RDMA approach to elucidate two-photon absorption (2PA) in indirect gap semiconductors, using silicon as the representative material. Our methodology, in contrast to existing models for 2PA in semiconductors, uniquely incorporates a detailed description of DTA (degenerate two-photon absorption) and NTA (non-degenerate two-photon absorption) through the production of excitons, a physical insight often overlooked in prior analyses. The approach allows the computation of the non-degenerate two-photon absorption coefficient, capturing the influence of both bound and free excitonic states within the material. In addition, the RDMA enables the inclusion of the effects of phonon-assisted transitions and material anisotropy. According to our model, the two-photon absorption process in silicon intensifies as the energy of individual incident photons, while below the gap, approaches the single bound excitonic state. This prediction aligns with recently obtained experimental NTA absorption data, shedding new light on the interpretation of published DTA data in bulk silicon. Above the gap, the 2PA process primarily occurs through the continuum of free states, providing a satisfactory description of the DTA data across a wide range of photon energies ($\hbar\omega/E_g = 0.5\text{--}1.3$). Finally, the analysis outlined using the RDMA can be generalized and readily applied to other indirect gap materials by adjusting the necessary material values. Furthermore, the model can be adapted to describe direct transitions by excluding the involvement of phonon modes to complete the transition.

SUPPLEMENTARY MATERIAL

The [supplementary material](#) provides further discussion on the extraction of the two-photon absorption coefficient from time-resolved data using pulse cross-correlation techniques.

ACKNOWLEDGMENTS

D.A.F. and E.O.P. acknowledged support of the Chan-Zuckerberg Initiative and the National Health Institute (Grant No. R21-GM141774). A.S. acknowledged support of the Air Force Office of Scientific Research (AFOSR) (Grant No. FA9550-23-1-0267). S.S.K. acknowledged support from the subsidy allocated to Kazan Federal University (Grant No. FZSM-2022-0021). A.I.N. acknowledged Kazan Federal University Strategic Academic Leadership Program (PRIORITY-2030).

AUTHOR DECLARATIONS

Conflict of Interest

The authors have no conflicts to disclose.

Author Contributions

David Ziemkiewicz: Conceptualization (equal); Data curation (equal); Formal analysis (equal); Investigation (equal); Methodology (equal); Project administration (equal); Supervision (equal); Validation (equal); Visualization (equal); Writing – original draft (equal); Writing – review & editing (equal). **David Knez:** Formal analysis (equal); Investigation (equal); Methodology (equal); Validation (equal); Writing – original draft (equal); Writing – review & editing (equal). **Evan P. Garcia:** Formal analysis (equal); Investigation (equal); Writing – review & editing (equal). **Sylwia Zielińska-Raczyńska:** Conceptualization (equal); Formal analysis (equal); Methodology (equal); Validation (equal); Writing – review & editing (equal). **Gerard Czajkowski:** Data curation (equal); Formal analysis (equal); Investigation (equal); Methodology (equal); Validation (equal); Writing – review & editing (equal). **Alessandro Salandrino:** Data curation (equal); Methodology (equal); Writing – review & editing (equal). **Sergey S. Kharintsev:** Data curation (equal); Methodology (equal); Writing – review & editing (equal). **Aleksei I. Noskov:** Formal analysis (equal); Methodology (equal); Writing – review & editing (equal). **Eric O. Potma:** Conceptualization (equal); Data curation (equal); Funding acquisition (equal); Investigation (equal); Methodology (equal); Resources (equal); Validation (equal); Writing – original draft (equal); Writing – review & editing (equal). **Dmitry A. Fishman:** Conceptualization (equal); Data curation (equal); Formal analysis (equal); Funding acquisition (equal); Investigation (equal); Methodology (equal); Project administration (equal); Resources (equal); Supervision (equal); Validation (equal); Visualization (equal); Writing – original draft (equal); Writing – review & editing (equal).

DATA AVAILABILITY

The data that support the findings of this study are available from the corresponding author upon reasonable request.

REFERENCES

- ¹W. Denk, J. H. Strickler, and W. W. Webb, "Two-photon laser scanning fluorescence microscopy," *Science* **248**, 73–76 (1990).
- ²S. Maruo, O. Nakamura, and S. Kawata, "Three-dimensional microfabrication with two-photon-absorbed photopolymerization," *Opt. Lett.* **22**, 132–134 (1997).
- ³S. Kawata, H. Sun, T. Tanaka, and K. Takada, "Finer features for functional microdevices," *Nature* **412**, 697 (2001).
- ⁴D. A. Parthenopoulos and P. M. Rentzepis, "Three-dimensional optical storage memory," *Science* **245**, 843–845 (1989).
- ⁵W. Rudolph, M. Sheik-Bahae, A. Bernstein, and L. F. Lester, "Femtosecond auto-correlation measurements based on two-photon photoconductivity in ZnSe," *Opt. Lett.* **22**, 313–315 (1997).
- ⁶S. Lochbrunner, P. Huppmann, and E. Riedle, "Crosscorrelation measurements of ultrashort visible pulses: Comparison between nonlinear crystals and SiC photodiodes," *Opt. Commun.* **184**, 321–328 (2000).
- ⁷D. A. Fishman, C. M. Cirloganu, S. Webster, L. A. Padilha, M. Monroe, D. J. Hagan, and E. W. Van Stryland, "Sensitive mid-infrared detection in wide-bandgap semiconductors using extreme non-degenerate two-photon absorption," *Nat. Photonics* **5**, 561–565 (2011).
- ⁸J. Fang, Y. Wang, M. Yan, E. Wu, K. Huang, and H. Zeng, "Highly sensitive detection of infrared photons by nondegenerate two-photon absorption under midinfrared pumping," *Phys. Rev. Appl.* **14**, 064035 (2020).
- ⁹D. Knez, A. M. Hanninen, R. C. Prince, E. O. Potma, and D. A. Fishman, "Infrared chemical imaging through non-degenerate two-photon absorption in silicon-based cameras," *Light: Sci. Appl.* **9**, 125 (2020).
- ¹⁰E. O. Potma, D. Knez, M. Eitenberg, M. Wizeman, H. Nguyen, T. Sudol, and D. A. Fishman, "High-speed 2D and 3D mid-IR imaging with an InGaAs camera," *APL Photonics* **6**, 096108 (2021).
- ¹¹W. Liu, D. Shen, G. Zhao, H. Yan, Z. Zhou, and W. Wan, "Spatial narrowing of two-photon imaging in a silicon CCD camera," *IEEE Photonics Technol. Lett.* **34**, 459–462 (2022).
- ¹²B. S. Wherrett, "Scaling rules for multiphoton interband absorption in semiconductors," *J. Opt. Soc. Am. B* **1**, 67 (1984).
- ¹³M. Sheik-Bahae, D. Hutchings, D. Hagan, and E. W. Van Stryland, "Dispersion of bound electron nonlinear refraction in solids," *IEEE J. Quantum Electron.* **27**, 1296–1309 (1991).
- ¹⁴D. C. Hutchings and E. W. Van Stryland, "Nondegenerate two-photon absorption in zinc blende semiconductors," *J. Opt. Soc. Am. B* **9**, 2065 (1992).
- ¹⁵G. Jalbert, B. Koiller, H. S. Brandi, and N. Zagury, "Dressed bands approach for multi-photon transitions in solids," *J. Phys. C: Solid State Phys.* **19**, 5745–5756 (1986).
- ¹⁶D. C. Hutchings and B. S. Wherrett, "Theory of anisotropy of two-photon absorption in zinc-blende semiconductors," *Phys. Rev. B* **49**, 2418–2426 (1994).
- ¹⁷C. Aversa, J. E. Sipe, M. Sheik-Bahae, and E. W. Van Stryland, "Third-order optical nonlinearities in semiconductors: The two-band model," *Phys. Rev. B* **50**, 18073–18082 (1994).
- ¹⁸C. Aversa and J. E. Sipe, "Nonlinear optical susceptibilities of semiconductors: Results with a length-gauge analysis," *Phys. Rev. B* **52**, 14636–14645 (1995).
- ¹⁹W.-R. Hannes and T. Meier, "Higher-order contributions and nonperturbative effects in the nondegenerate nonlinear optical absorption of semiconductors using a two-band model," *Phys. Rev. B* **99**, 125301 (2019).
- ²⁰M. Dinu, "Dispersion of phonon-assisted nonresonant third-order nonlinearities," *IEEE J. Quantum Electron.* **39**, 1498–1503 (2003).
- ²¹M. Dinu, F. Quochi, and H. Garcia, "Third-order nonlinearities in silicon at telecom wavelengths," *Appl. Phys. Lett.* **82**, 2954–2956 (2003).
- ²²A. Hayat, P. Ginzburg, and M. Orenstein, "Infrared single-photon detection by two-photon absorption in silicon," *Phys. Rev. B* **77**, 125219 (2008).
- ²³S. Faryadras, N. Cox, D. J. Hagan, and E. W. Van Stryland, "Non-degenerate two-photon absorption spectroscopy of bulk silicon," in *2021 IEEE Research and Applications of Photonics in Defense Conference (RAPID)* (IEEE, 2021), pp. 1–2.
- ²⁴S. Zielińska-Raczyńska, G. Czajkowski, K. Karpiński, and D. Ziemkiewicz, "Nonlinear optical properties and self-Kerr effect of Rydberg excitons," *Phys. Rev. B* **99**, 245206 (2019).
- ²⁵C. Morin, J. Tignon, J. Mangeney, S. Dhillon, G. Czajkowski, K. Karpiński, S. Zielińska-Raczyńska, D. Ziemkiewicz, and T. Boulter, "Self-Kerr effect across the yellow Rydberg series of excitons in Cu₂O," *Phys. Rev. Lett.* **129**, 137401 (2022).
- ²⁶H. Haug and S. Schmitt-Rink, "Basic mechanisms of the optical nonlinearities of semiconductors near the band edge," *J. Opt. Soc. Am. B* **2**, 1135–1142 (1985).
- ²⁷F. Bechstedt and S. Glutsch, "Non-equilibrium screening and plasmons in a coherently pumped semiconductor," *J. Phys.: Condens. Matter* **3**, 7145 (1991).
- ²⁸A. Stahl, "Electrodynamics of the band-edge in a direct gap semiconductor," *Solid State Commun.* **49**, 91–93 (1984).
- ²⁹G. Czajkowski, F. Bassani, and L. Silvestri, "Excitonic optical properties of nanostructures: Real density matrix approach," *Riv. Nuovo Cimento* **26**, 1–150 (2003).
- ³⁰V. Axt and A. Stahl, "The role of the biexciton in a dynamic density matrix theory of the semiconductor band edge," *Z. Phys. B: Condens. Matter* **93**, 205–211 (1994).
- ³¹"Silicon (Si), band structure," in *Semiconductors—Group IV Elements, IV-IV and III-V Compounds. Part b - Electronic, Transport, Optical and Other Properties* Landolt-Börnstein—Group III Condensed Matter Vol. 41A1β, edited by O. Madelung, U. Rössler, and M. Schulz (Springer-Verlag, Berlin, Heidelberg, 2002), https://materials.springer.com/lb/docs/sm_lbs_978-3-540-31356-4_432.
- ³²A. Stahl, "RPA-dynamics of the electronic density matrix in a two-band semiconductor," *Z. Phys. B: Condens. Matter* **72**, 371–377 (1988).
- ³³W. Huhn and A. Stahl, "Self-consistent field theory applied to the semiconductor band edge," *Phys. Status Solidi B* **124**, 167–177 (1984).
- ³⁴A. Stahl and I. Balslev, *Electrodynamics of the Semiconductor Band Edge* (Springer-Verlag, Berlin, Heidelberg, New York, 1987).
- ³⁵A. Stahl, "Coupled two-level systems and the dynamics of semiconductor electrons," *Phys. Status Solidi B* **159**, 327–337 (1990).
- ³⁶V. M. Axt and S. Mukamel, "Nonlinear optics of semiconductor and molecular nanostructures; a common perspective," *Rev. Mod. Phys.* **70**, 145–174 (1998).
- ³⁷F. Bassani and G. P. Parravicini, *Electronic States and Optical Transitions in Solids* (Pergamon Press, Oxford, 1975).
- ³⁸A. Valentin, J. Sée, S. Galdin-Retailleau, and P. Dollfus, "Study of phonon modes in silicon nanocrystals using the adiabatic bond charge model," *J. Phys.: Condens. Matter* **20**, 145213 (2008).
- ³⁹D. S. Kim, H. L. Smith, J. L. Niedziela, C. W. Li, D. L. Abernathy, and B. Fultz, "Phonon anharmonicity in silicon from 100 to 1500 K," *Phys. Rev. B* **91**, 014307 (2015).
- ⁴⁰S. Zielińska-Raczyńska, D. Ziemkiewicz, and G. Czajkowski, "Electro-optical properties of Rydberg excitons," *Phys. Rev. B* **94**, 045205 (2016).
- ⁴¹M. A. Green, "Improved value for the silicon free exciton binding energy," *AIP Adv.* **3**, 112104 (2013).
- ⁴²D. Frank and A. Stahl, "Nonlinear susceptibility $\chi^{(3)}$ in a direct gap semiconductor derived from coupled inter- and intraband equations of motion," *Solid State Commun.* **52**, 861–865 (1984).
- ⁴³W. H. Strehlow and E. L. Cook, "Compilation of energy band gaps in elemental and binary compound semiconductors and insulators," *J. Phys. Chem. Ref. Data* **2**, 163–200 (1973).
- ⁴⁴B. Venitucci and Y.-M. Niquet, "Simple model for electrical hole spin manipulation in semiconductor quantum dots: Impact of dot material and orientation," *Phys. Rev. B* **99**, 115317 (2019).
- ⁴⁵D. Palmer, www.semiconductors.co.uk.
- ⁴⁶J. Singh, *Physics of Semiconductors and Their Heterostructures*, McGraw-Hill Series in Electrical and Computer Engineering (McGraw-Hill, New York, 1993).
- ⁴⁷R. Negres, J. Hales, A. Kobaykov, D. Hagan, and E. W. Van Stryland, "Experiment and analysis of two-photon absorption spectroscopy using a white-light continuum probe," *IEEE J. Quantum Electron.* **38**, 1205–1216 (2002).
- ⁴⁸A. D. Bristow, N. Rotenberg, and H. M. van Driel, "Two-photon absorption and Kerr coefficients of silicon for 850–2200 nm," *Appl. Phys. Lett.* **90**, 191104 (2007).
- ⁴⁹H. Garcia and R. Kalyanaraman, "Phonon-assisted two-photon absorption in the presence of a DC-field: The nonlinear Franz-Keldysh effect in indirect gap semiconductors," *J. Phys. B: At., Mol. Opt. Phys.* **39**, 2737 (2006).